Neuroscience, Structural Biology and Molecular Biophysics

Molecular tuning of sea anemone stinging

Reviewed Preprint

Published from the original preprint after peer review and assessment by eLife.

About eLife's process

Reviewed preprint posted
July 5, 2023 (this version)

Posted to bioRxiv
June 16, 2023

Sent for peer review
May 4, 2023

Lily S He, Yujia Qi, Corey AH Allard, Wendy A Valencia-Montoya, Stephanie P Krueger, Keiko Weir, Agnese Seminara , Nicholas W Bellono

Department of Molecular and Cellular Biology, Harvard University, Cambridge MA 02138 USA • Machine Learning Center Genoa (MalGa), Department of Civil, Chemical and Environmental Engineering (DICCA), University of Genoa, Via Montallegro 1, 16145 Genoa, Italy • Department of Organismic and Evolutionary Biology and Museum of Comparative Zoology, Harvard University, Cambridge MA 02138 USA

Abstract

Jellyfish and sea anemones fire single-use, venom-covered barbs to immobilize prey or predators. We previously showed that the anemone *Nematostella vectensis* uses a specialized voltage-gated calcium (Ca_V) channel to trigger stinging in response to synergistic prey-derived chemicals and touch (Weir et al., 2020). Here we use experiments and theory to find that stinging behavior is suited to distinct ecological niches. We find that the burrowing anemone *Nematostella* uses uniquely strong Ca_V inactivation for precise control of predatory stinging. In contrast, the related anemone *Exaiptasia diaphana* inhabits exposed environments to support photosynthetic endosymbionts. Consistent with its niche, *Exaiptasia* indiscriminately stings for defense and expresses a Ca_V splice variant that confers weak inactivation. Chimeric analyses reveal that $Ca_V\beta$ subunit adaptations regulate inactivation, suggesting an evolutionary tuning mechanism for stinging behavior. These findings demonstrate how functional specialization of ion channel structure contributes to distinct organismal behavior.

eLife assessment

This is an **important** paper that links distinctive stinging behavior of two related anemones occupying different ecological niches to varying inactivation properties of voltage-gated calcium channels conferred by auxiliary Cavβ subunits. Further **convincing** evidence is provided that these differences are mediated by alternative splicing of Cavβ subunit of the calcium channel. The study will be of interest to scientists studying Ca2+ signaling, ion channel biophysicists, and marine biologists.

Introduction

Sea anemones, jellyfish, corals, and hydrozoans of the Cnidarian phylum use specialized cells called nematocytes to sting for predation or defense. Mechanical and chemical stimuli from prey or predators act synergistically on nematocytes to mediate rapid discharge of a toxin-covered barb from its nematocyst organelle (Holstein and Tardent, 1984; Watson and

Mire-Thibodeaux, 1994; Babonis and Martindale, 2014). Nematocyst discharge requires calcium (Ca^{2+}) influx and, as a one-time use organelle, is tightly controlled to prevent energetically wasteful stinging to irrelevant stimuli (Lubbock et al., 1981; Gitter et al., 1994; Watson and Hessinger, 1994). We previously found that the starlet sea anemone *Nematostella vectensis* uses a uniquely adapted voltage-gated Ca^{2+} channel (Ca_V) to integrate simultaneously presented chemical and mechanical cues that elicit nematocyst discharge. Unusually strong voltage-dependent inactivation of *Nematostella* Ca_V prevents stinging responses to extraneous, non-prey touch signals by reducing and preventing cellular excitability. Ca_V inactivation is relieved by hyperpolarization of the nematocyte membrane potential to very negative voltages through the effect of prey-derived chemosensory signals that are synaptically transmitted from sensory neurons. Upon relieving Ca_V inactivation, direct touch responses are amplified to trigger nematocyst discharge (Weir et al., 2020). Thus, single nematocytes integrate synergistic cues to elicit a precise response, representing a unique cellular system to study how cells detect and transduce signals to produce discrete behavior.

While Ca_V-mediated sensory integration represents one mechanism by which nematocytes "decide" when to sting, the incredible diversity of cnidarian biology suggests that stinging behavior must be adapted to support the demands of different lifestyles. Cnidarian taxa occupy diverse environmental niches and endure specific metabolic demands, predatory challenges, and environmental pressures for survival, which results in distinct selective pressures on nematocyte evolution (Beckmann and Özbek, 2012; Babonis et al., 2022). *Nematostella vectensis* and *Exaiptasia diaphana* represent an example of closely related cnidarians with differing environmental niches and metabolic demands (Darling et al., 2005; Bedgood et al., 2020). *Nematostella* are found in shallow brackish water of coastal marshes where they are buried in the mud, hidden from predators, with only their tentacles exposed to catch unsuspecting passing prey (Fraune et al., 2016). Thus, we hypothesize that their stinging is under tight regulation adapted for opportunistic predation. In contrast, *Exaiptasia* are exposed to predators while living in shallow, open ocean environments that provide sufficient sunlight for their endosymbionts to produce important photosynthetic products and nutrients (Baumgarten et al., 2015). Considering these dramatically different ecological contexts, we hypothesized that Ca_V-mediated regulation of nematocyte discharge has adapted to reflect the demands on stinging behavior in these two anemones. We therefore probed the behavior of these related but distinct anemones and investigated how subtle tuning of a shared molecular-regulatory mechanism drives adaptation in physiology and behavior associated with niche diversification.

In this study, we find that the symbiotic anemone *Exaiptasia* stings in response to mechanical stimuli alone, independent of predation pressure. This behavior serves as a stark contrast with *Nematostella* stinging, which is only elicited by synergistic prey chemicals and touch. Markov decision process modeling coupled with behavioral experiments revealed that *Nematostella* stings as an optimal predator, whereas *Exaiptasia* exhibits optimal defensive stinging behavior. Consistent with indiscriminate stinging behavior, we discover that *Exaiptasia* nematocyte physiology lacks the unusual Ca_V inactivation used by *Nematostella* to prevent responses to touch in the absence of prey chemicals. Weak inactivation of *Exaiptasia* Ca_V is mediated by a splice isoform of the beta subunit ($Ca_V\beta$) with a distinct N-terminus. Analysis of chimeric jellyfish and anemone channels reveals that Ca_V inactivation is broadly regulated by the $Ca_V\beta$ N-terminus, suggesting an evolutionary tuning mechanism that could contribute to specific stinging behavior across cnidarians. Thus, we propose Ca_V adaptations as one molecular mechanism that could shift predatory versus defensive stinging in cnidarians. These results highlight how subtle adaptations in protein structure contribute to complex organismal behavior.

Results

Comparative sea anemone stinging behavior

In their natural habitat, *Nematostella* are hidden by burrowing within the sandy substrate and use an opportunistic predatory strategy to capture prey with their tentacles. In contrast, symbiotic *Exaiptasia* are found within open waters where they experience greater risk of predation and therefore must adopt a more defensive stance. Thus, we first asked whether differences in ecological pressure are reflected by stinging behavior. Consistent with our previous findings, we observed *Nematostella* stinging in response to simultaneously delivered prey extract and touch, reflecting stinging control adapted for predation (**Figure 1**) (Weir et al., 2020). Strikingly, *Exaiptasia* tentacles instead exhibited robust stinging even in the absence of prey chemicals (touch alone, **Figure 1**). Similar touch-evoked stinging was observed for *Exaiptasia* acontia, which are defensive nematocyte-enriched structures that are ejected and release toxins to repel predators (Lam et al., 2017). Considering the drastic differences in stinging behavior, we wondered if *Exaiptasia*'s indiscriminate stinging reflects a distinct control strategy.

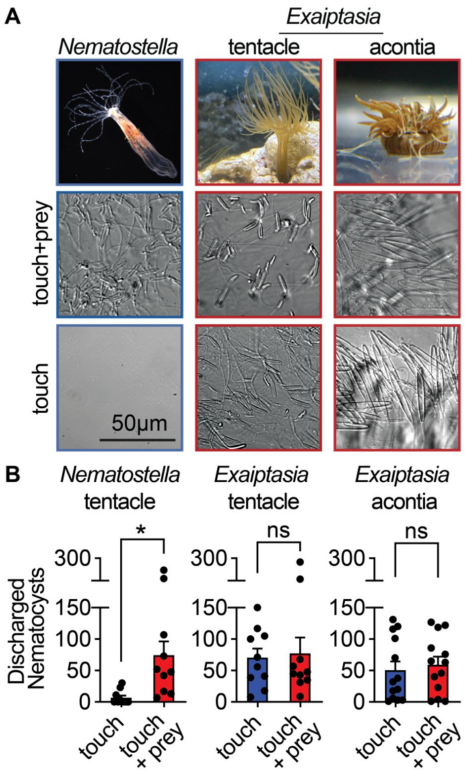

Figure 1.

Comparative sea anemone stinging behavior.

A) *Nematostella vectensis* stings with tentacles while *Exaiptasia diaphana* also stings with acontia filaments that are ejected from its body for defense. *Left*: *Nematostella* nematocyte discharge was only observed in response to simultaneous prey chemicals and touch stimuli. *Middle, Right*: *Exaiptasia* nematocyte discharge from tentacles and acontia occurred irrespective of prey cues (touch alone). Scale bar = 50μm.

B) *Nematostella* nematocyte discharge was elicited by simultaneous touch and prey chemical stimuli (n = 10 trials). *Exaiptasia* tentacle (n = 10) and acontia (n = 13) nematocytes discharged only to touch, with or without prey chemicals. $p < 0.05$ for *Nematostella*, paired two-tailed student's t-test. Data represented as mean ± sem.

To investigate whether different stinging behaviors might be suited for predation versus defense, we developed a normative theory aimed at predicting optimal stinging behavior as a function of nutritional state (see ***Supplementary Information*** for model details). We focused on stinging intensity, defined as the fraction of nematocysts discharged during a stinging event, and asked whether nutritional state would affect optimal predatory and defensive stinging. In the language of decision models, the intensity of stinging is an action, and it is chosen by the agent, or anemone. In our study, "choice" of stinging means modulation of behavior with nutritional state, rather than a cognitive process. Each choice has associated costs and benefits that depend on the environment. Because anemones sting

many times over the course of their lives, an optimal behavior must account for overall costs and benefits after many events; therefore, this is a sequential decision-making problem.

We modeled the optimal stinging response to a given environment by using Markov decision processes (MDP). Each anemone was modeled as an "agent" that must hedge the intensity of its stinging response. The environment, including the identity of prey, predators, and the physiological state of the animals, defines the likelihood, costs, and benefits of successful stinging. Specifically, intense stinging responses are costly since each fired nematocyst needs to be regenerated. But they are also more likely to succeed because greater discharge of stinging barbs increases the likelihood of contact and envenomation. The cost per nematocyte was assumed to be constant and equivalent for defensive and predatory stinging as nematocyst discharge requires regeneration in either case. We assumed that the benefits of successful predatory stinging depend on the capture and consumption of prey, which improves satiation. In contrast, stinging a predator for defense would not improve nutritional state, hence the benefits of stinging would not depend on satiation. We then used the model to predict optimal stinging that maximizes benefits while minimizing costs during starvation and tested the prediction directly against experiments with behaving animals.

Using this approach, we found that optimal stinging strategies were completely different for predatory versus defensive behavior. Regardless of the specific environment (likelihood to succeed and specific costs and benefits), predatory stinging increased with starvation (**Figure 2A**, **2B**). To test our theory regarding predatory stinging, we carried out simulations in which agents discharged a random fraction of nematocytes between 0 and 1, regardless of starvation. Random stinging was unsustainable over numerous events and agents quickly reached maximal starvation state. Agents using optimal predatory stinging discharged more nematocysts when starved and less when satiated, leading to sustained stinging behavior and survival. This was true even if they fired the same fraction of nematocytes as the random agent (**Figure 2C**). In contrast, optimal stinging for defense stayed constant or decreased with starvation (**Figure 2D**, **2E**). Importantly, while the precise optimal response depended on the details of cost and reward that defined the MDP, the differences between predatory versus defensive stinging were consistent and largely independent of assumptions associated with each reward function (**Figure 2B and 2E**). These results reflect greater rewards to predatory anemones upon stinging during starvation, whereas defensive anemones sting at a similar rate regardless of nutritional status. Thus, our model predicts robust differences in predatory versus defensive stinging behavior.

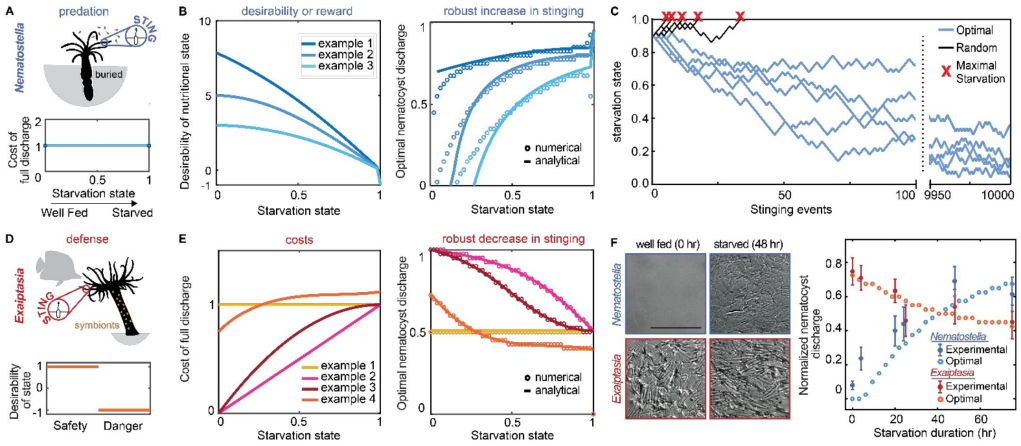

Figure 2.

Nematostella stinging is regulated by predation while *Exaiptasia* stings for defense.

A) *Top: Nematostella* burrows in the substrate and stings for predation. *Bottom*: We assumed the cost of stinging does not change with starvation state.

B) *Left*: Desirability of nutritional state, or reward, decreases with starvation. Three examples are shown: example 1, $r(s) = 10\ tan^{-1}(1 - s)$; example 2, $r(s) = 5\cos\left(\frac{s\pi}{2}\right)$; and example 3, $r(s) = 3 - 3s^2$. *Right*: Predicted optimal stinging obtained by solving equation (1) with numerical simulations (circles) and approximate analytical solutions (lines) assuming $p(a) = p_M\, a(2-a)$ and $p_M = 0.8$ and $c = c_0 a$ with a constant cost for full discharge $c_0 = 1$. Colors match the corresponding reward in Left panels. For all three reward functions, optimal predatory stinging increases with starvation under broad assumptions (*see* ***Supplementary Information***).

C) Examples of optimal (blue) versus random (black) predatory stinging. Each agent (anemone) starts with $s = 0.9$, and stings sequentially for many events (represented on the x axis). The random agent almost always reaches maximal starvation before time 50 events (grey lines, five examples shown). In comparison, the optimal agent effectively never starves due to a successful stinging strategy optimized for predation (blue lines, five examples shown, parameters as in panel B, curve with matching color).

D) *Top: Exaiptasia diaphana* relies heavily on endosymbiotic algae for nutrients and stings primarily for defense. *Bottom*: We assumed there are two states, safety (L), and danger (D). The state of safety can transition to danger, but not the other way around. We assumed the agent obtains reward 1 in state L and penalty −1 in state D.

E) *Left*: Cost function, which is assumed to increase linearly with the fraction of nematocysts discharged $c_s(a) = c_0 a$ The cost c_0 for full discharge is constant as in panel A, $c_0 = 1$ (example 1), or varies with starvation: $c_0(s) = s$ (example 2), $c_0(s) = 1 - (s - 1)^2$ (example 3) and c_0 obtained by fitting the experimental data (example 4) (*see fitting procedure in* ***Supplementary Information***). *Right*: Predicted optimal stinging obtained by solving equation (2) with numerical simulations (circles) and analytical solutions (lines). Colors match the corresponding cost in Left panels, and we assume $p(a) = P_M\, a(2 - a)$ and $p_M = 0.8$ as before. Optimal defensive stinging is constant or decreases with starvation under broad assumptions (*see* ***Supplementary Information***).

F) *Left: Nematostella* nematocyte discharge was affected by prey availability while *Exaiptasia* stung at a similar rate regardless of feeding. $p < 0.0001$ for *Nematostella*, two-way ANOVA with post hoc Bonferroni test (n = 10 animals, data represented as mean ± sem). *Right*: Normalized optimal nematocyst discharge predicted from MDP models for both *Exaiptasia* (orange circles, using the cost function in E, example 4) and *Nematostella* (blue circles, using the reward function in B, example 2) fit the experimental measurements well. We match the last experimental data point to $s = 0.5$, the precise value of this parameter is irrelevant as long as it is smaller than 1, representing that animals are not severely starved during the experiment.

We next sought to experimentally test whether pressure to predate regulates stinging in *Nematostella* and *Exaiptasia*. To do so, we fed both species of anemones copious amounts of prey (brine shrimp, *Artemia nauplii*) for 1-2 weeks and then deprived them of food for 5 days. Following manipulation of prey availability, *Nematostella* significantly increased stinging in response to starvation, while *Exaiptasia* stinging remained relatively constant despite complete deprivation of prey (**Figure 2F**). The behavior was remarkably consistent with our normative theory of optimal stinging strategies for predation versus defense (**Figure 2F**). Furthermore, changes in *Nematostella* and *Exaiptasia* stinging were not due to changes in the abundance of nematocytes because tentacles from both animals were abundantly armed with nematocytes across feeding conditions (**Figure 2S1A**). Thus, we conclude that *Nematostella* controls stinging for opportunistic predation while *Exaiptasia* stinging is indiscriminate and serves a greater defensive role for this symbiotic anemone.

Sea anemones with different stinging behavior use distinct Ca_V channels

We next probed the physiological basis underlying these significantly different stinging behaviors. We previously found that *Nematostella* stinging is triggered by a specialized Ca_V channel that exhibits strong inactivation to prevent responses to extraneous non-prey mechanical stimuli (Weir et al., 2020). Ca^{2+} influx triggers an increase in hydrostatic pressure inside the nematocyst capsule that forces the stinging thread to evert explosively at an acceleration of up to 5.41×10^6g, placing it among the fastest biological processes in existence (Lubbock and Amos, 1981; Lubbock et al., 1981; Holstein and Tardent, 1984; Weber, 1990; Gitter et al., 1994; Tardent, 1995; Nüchter et al., 2006). Similar to *Nematostella*, *Exaiptasia* stinging required extracellular Ca^{2+} and was abolished by Cd^{2+}, a Ca_V channel blocker (**Figure 3A**). Consistent with a Ca^{2+}-dependent stinging mechanism, whole-cell patch clamp recordings from nematocytes revealed the presence of voltage-gated inward currents that were blocked by Cd^{2+}, suggesting that *Exaiptasia* nematocytes also use Ca_V channels to control stinging (**Figure 3B**). Indeed, Ca_V currents in *Exaiptasia* nematocytes exhibited similar voltage-dependent activation properties compared with *Nematostella* nematocytes (**Figure 3C**). Thus, in agreement with previous findings, we conclude that Ca^{2+} influx via Ca_V channels is broadly important for stinging.

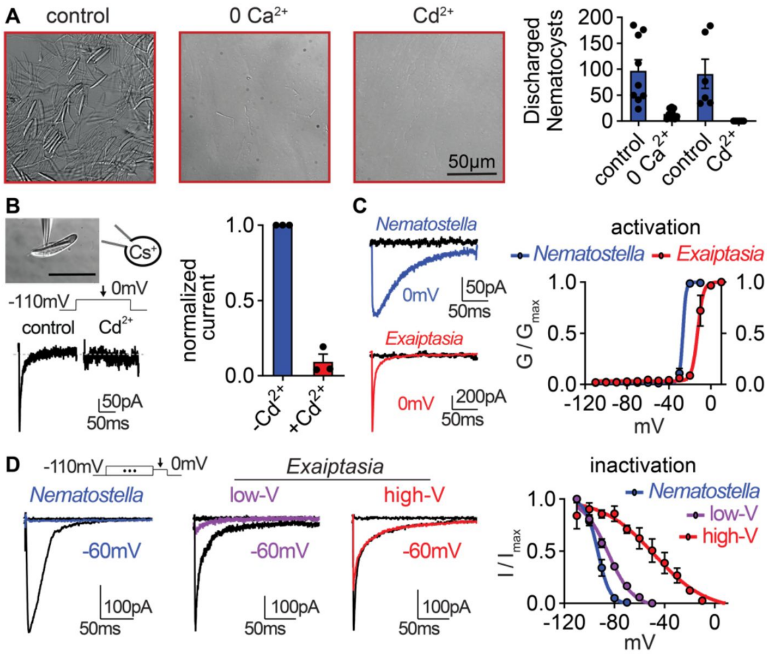

Figure 3.

Exaiptasia nematocyte voltage-gated Ca^{2+} currents have weak inactivation compared with *Nematostella*.

A) Touch-elicited *Exaiptasia* tentacle nematocyte discharge was blocked in the absence of Ca^{2+} ($p < 0.01$, paired two-tailed student's t-test, n = 9) or by addition of the Ca_V channel blocker Cd^{2+} (500µM, $p < 0.05$, paired two-tailed student's t-test, n = 6). Scale bar = 50µm.

B) *Top:* Representative patch clamp experiment from an *Exaiptasia* nematocyte. Scale bar = 20µm. *Bottom*: Nematocyte voltage-gated currents elicited by a maximally activating 0mV pulse were blocked by Cd^{2+} (n = 3, $p < 0.01$, paired two-tailed student's t-test).

C) Nematocyte voltage-gated currents elicited by −120mV (black) or 0mV pulses (colored). Conductance-voltage curves for *Nematostella* nematocyte ($V_{a1/2}$ = −26.54 ± 0.78mV, n = 3) and *Exaiptasia* nematocyte ($V_{a1/2}$ = −12.47 ± 0.70mV, n = 3).

D) Nematocyte voltage-gated currents elicited by a maximally activating voltage pulse following 1 s pre-pulses to −110 mV (max current, black), −50 mV (colored), or 20 mV (inactivated, no current). *Nematostella* nematocytes inactivated at very negative voltages ($V_{i1/2}$ = −93.22 ± 0.42mV, n = 7) while *Exaiptasia* contained two populations of nematocytes: low-voltage threshold ($V_{i1/2}$ = −84.94 ± 0.70mV, n = 4), and high-voltage threshold ($V_{i1/2}$ = −48.17 ± 3.32mV, n = 3). Data represented as mean ± sem.

Ca_V channels respond to positive membrane potentials by opening to conduct Ca^{2+}. However, sustained positive voltage drives Ca_Vs to transition to a non-conducting state (inactivation) that prevents re-activation until channels return to a resting state induced by negative membrane potentials. In most cells, voltage-gated ion channel inactivation prevents extended responses to repetitive or prolonged stimulation. *Nematostella* Ca_V, is unusual because it inactivates at very negative voltages to prevent responses from resting potential, resulting in nematocytes that cannot fire from rest (Weir et al., 2020). In contrast to *Nematostella* nematocytes in which half of all Ca_V channels ($V_{i1/2}$) were inactivated at ~ −93mV, *Exaiptasia* nematocytes exhibited two distinct inactivation phenotypes: (1) nematocytes with low-voltage threshold (low-V) inactivation similar to that of *Nematostella* (low-V, $V_{i1/2}$ = ~ −85mV); and (2) a distinct population with weak, high-voltage (high-V) threshold inactivation (high-V, $V_{i1/2}$ = ~ −48mV) (**Figure 3D**). While we did not observe a correlation with abundance or distinct cellular morphology (Östman, 2000; Kass-Simon and Scappaticci, 2002; Grajales and Rodríguez, 2014), we could clearly distinguish the two populations based on these electrophysiological features. Importantly, high-V nematocyte inactivation was minimal at resting voltages (~ −70mV), so nearly all channels would be available to amplify depolarizing signals, such as those elicited by touch. Thus, these markedly different physiological properties correlate with distinct stinging behavior: *Nematostella* uses unusual Ca_V inactivation to integrate sensory cues for tightly regulated

predatory stinging. In contrast, *Exaiptasia* employs a population of nematocytes with weak Ca_V inactivation, consistent with direct activation from resting potentials and stinging to touch alone.

What is the molecular basis of distinct nematocyte physiology? Ca_V channels are made of at least three subunits: the pore-forming α and auxiliary β and α2δ subunits. Transcriptomics revealed that nematocyte-enriched tentacles of *Exaiptasia* expressed *cacna1a*, the pore-forming subunit homologous to that of the previously characterized *Nematostella* nematocyte Ca_V channel (**Figure 4S1**). We also analyzed the Ca_V β subunit, Ca_Vβ, which is required and sufficient for the unusual inactivation properties observed in *Nematostella* Ca_V (Weir et al., 2020) (**Figure 4S1**). From *Exaiptasia*, we identified two isoforms of Ca_Vβ: $EdCa_V$β1 and $EdCa_V$β2. Droplet digital PCR assays of mRNA abundance showed that both isoforms are expressed throughout *Exaiptasia* tissues, suggesting they could both be functionally important (**Figure 4A**, **4S1B**). To localize Ca_Vβ, we used *in situ* hybridization to determine that distinct nematocyte populations expressed either $EdCa_V$β1 or $EdCa_V$β2 mRNA (but not both) in the same cell (**Figure 4B**).

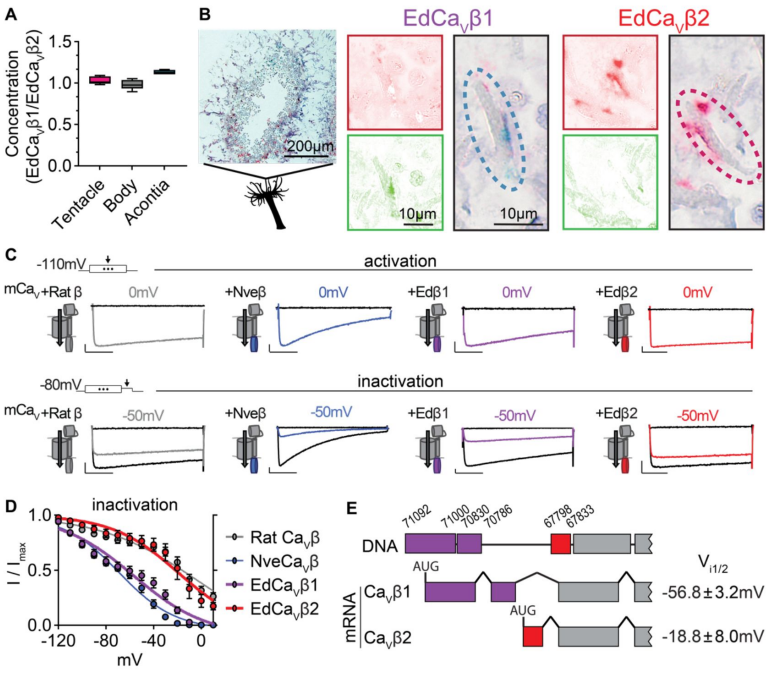

Figure 4.

Exaiptasia expresses a Ca_V β subunit splice isoform that confers weak voltage-dependent inactivation.

A) ddPCR ratio of concentrations of Ca_V β subunit 1 and 2 mRNAs was similar in tentacle (n = 5), body (n = 5), and acontia (n = 4 animals) tissue samples.

B) $EdCa_V$β1 and $EdCa_V$β2 localized to distinct nematocytes in *Exaiptasia* tentacle cross section, as visualized by BaseScope *in situ* hybridization. Representative nematocyte expressing $EdCa_V$β1 (green) or $EdCa_V$β2 (red). Representative of 3 animals.

C) Voltage-gated currents from heterologously-expressed chimeric mammalian Ca_V (mCa_V) with different β subunits: rat (*Rattus norvegicus*), *Nematostella* (Nve), *Exaiptasia* $EdCa_V$β1 or $EdCa_V$β2. *Top*: Currents elicited by voltage pulses to −120mV (no current, black) and maximally activating 0mV (colored). *Bottom*: Voltage-gated currents elicited by a maximally activating voltage pulse following 1 s pre-pulses to −110 mV (max current, black), −50 mV (colored), or 20 mV (inactivated, no current, black). Scale bars = 100pA, 50ms.

D) *Exaiptasia* Ca_V β subunit splice isoforms confer distinct inactivation: *Nematostella* β subunit ($V_{i1/2}$ = −68.93 ± 1.53mV, n = 5) and Rat β subunit ($V_{i1/2}$ = −2.98 ± 13.51mV, n = 12) and $EdCa_V$β1 ($V_{i1/2}$ = - 56.76 ± 3.18mV, n = 8), and $EdCa_V$β2 ($V_{i1/2}$ = −18.84 ± 8.00mV, n = 5). Data represented as mean ± sem.

E) Genomic alignment of *Exaiptasia* β subunit isoforms showed that alternative splicing of the N-terminus region was associated with distinct inactivation: Ca_Vβ1 (long N-term) had strong inactivation similar to *Nematostella*, while Ca_Vβ2 (short N-term) exhibited weak inactivation similar to its mammalian orthologue. Genomic loci listed above genomic sequence.

Considering this expression profile, we wondered if the two $Ca_V\beta$ isoforms could mediate low-V and high-V inactivation phenotypes in *Exaiptasia* nematocytes. To investigate this question, we heterologously expressed each β subunit isoform with other well-characterized Ca_V subunits (mammalian Ca_V α and α2δ) that express well in heterologous systems. Both channels exhibited functional Ca_V currents with similar activation thresholds (**Figure 4C**). However, $EdCa_V\beta1$- and $EdCa_V\beta2$-containing channels significantly differed in their inactivation properties. $EdCa_V\beta1$ inactivated at negative voltages, similar to channels containing *Nematostella* $Ca_V\beta$ ($NveCa_V\beta$). In contrast, $EdCa_V\beta2$ mediated Ca_V currents with weak inactivation, more like channels containing rat $Ca_V\beta$ (**Figure 4C**, **D**). Thus, $EdCa_V\beta1$ and $EdCa_V\beta2$ confer strong and weak inactivation, respectively, and are expressed in distinct nematocytes, consistent with low-V and high-V threshold inactivating nematocyte populations. Genomic alignment revealed that alternative splicing at the N-terminus gives rise to $EdCa_V\beta1$ and $EdCa_V\beta2$ isoforms, serving as a mechanism to dynamically tune nematocyte physiology and potentially stinging behavior in contrast to adaptation through gene duplication and divergence (**Figure 4E**). Furthermore, by expressing two functional variants, *Exaiptasia* could use distinct nematocyte populations for different behaviors, including a less pronounced role for predation.

Structural adaptations across cnidarian Ca_V channels

We next asked how variation in $Ca_V\beta$ structure mediates strong phenotypes by testing whether distinct protein domains confer low or high voltage-dependent inactivation. We first compared rat and *Nematostella* $Ca_V\beta$s ($NveCa_V\beta$), which have significantly different voltage-dependent properties (Weir et al., 2020). Swapping the well-characterized SH3, HOOK, and GK domains had no effect on inactivation, but the $NveCa_V\beta$ N-terminus was both required and sufficient for low voltage-dependent inactivation (**Figure 5A**, **B**). Indeed, swapping only the N-terminus of $NveCa_V\beta$ was sufficient to shift rat inactivation by ~ −75mV (**Figure 5A**, **B**). This finding is consistent with the variation in $EdCa_V\beta$ splice isoforms, in which differences in the N-terminus account for a ~ 40mV difference in inactivation thresholds.

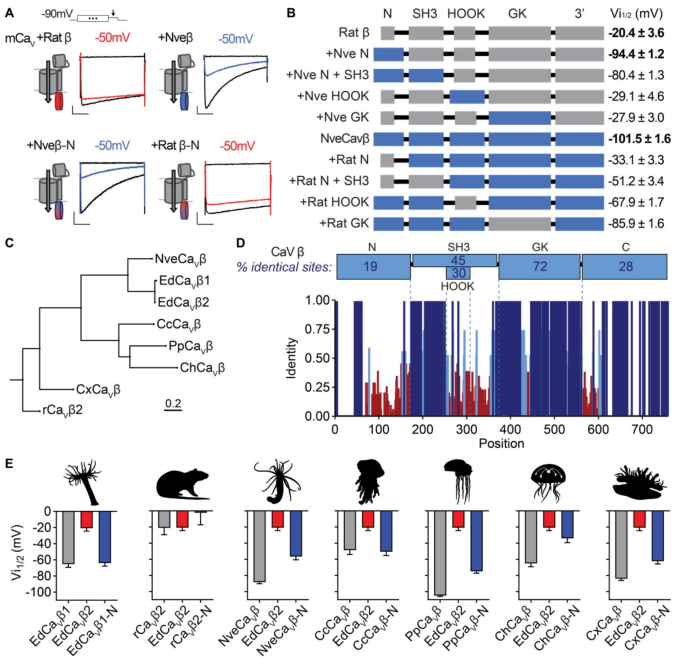

Figure 5.

Cnidarian Ca_V β subunit N-termini confer unique inactivation properties.

A) Voltage-gated currents from heterologously expressed Ca_V channels with *Nematostella*-rat chimeric β subunits demonstrate that the *Nematostella* N-terminus is sufficient to drive inactivation at negative voltages. Currents shown in response to 10 mV voltage pulses following 1 s pre-pulses to −130 mV (max current, black), −50 mV (colored), or 0 mV (inactivated, no current, black). Scale bars = 100pA, 50ms.

B) Diagram of Ca_V *Nematostella*-rat β subunit domain swaps and resulting $V_{i1/2}$ values. The *Nematostella* β subunit N-terminus is required and sufficient for uniquely hyperpolarized Ca_V inactivation properties ($p < 0.001$ for average $V_{i1/2}$ values across mutant beta

subunits, one-way ANOVA with post-hoc Tukey test, n = 2-8 cells).

C) Phylogenetic tree of β subunit sequences obtained from several species of cnidarians. Abbreviations of species: Nve, *Nematostella vectensis*; Ed, *Exaiptasia diaphana*; Cc, *Cyanea capillata* (jellyfish); Pp, *Physalia physalis* (siphonophore); Ch, *Clytia hemisphaerica* (jellyfish); Cx, *Cassiopea xamachana* (jellyfish); r, *Rattus norvegicus*.

D) *Top*: Percentage of identity between amino acid sequences across β subunit protein domains for NveCa_Vβ, EdCa_Vβ1, EdCa_Vβ2, CcCa_Vβ, PpCa_Vβ, ChCa_Vβ, CxCa_Vβ2, rCa_Vβ2. *Bottom*: Fraction of identity of amino acids across sites of the β subunit protein.

E) Cnidarian Ca_V β N-termini shift weak voltage-dependent inactivation of Ca_V channels containing EdCa_Vβ2. Voltage-dependent inactivation ($V_{i1/2}$) of heterologously-expressed Ca_Vs with WT EdCa_Vβ2, β subunits from the indicated cnidarians, and chimeras with their N-termini on EdCa_Vβ2 ($p < 0.0001$ for average $V_{i1/2}$ values with multiple comparisons against WT EdCa_Vβ2 mean, one-way ANOVA with Bartlett's test and post-hoc Tukey test, n = 4-9 cells). Data represented as mean ± sem.

To explore evolutionary relationships of Ca_Vβ, we constructed a phylogenetic tree of sequences from various cnidarians including *Nematostella vectensis* (anemone, NveCa_Vβ), *Exaiptasia diaphana* (anemone, EdCa_Vβ1 and EdCa_Vβ2), *Cyanea capillata* (jellyfish, CcCa_Vβ), *Physalia physalis* (hydrozoan, PpCa_Vβ), *Clytia hemisphaerica* (jellyfish, ChCa_Vβ), *Cassiopea xamachana* (jellyfish, CxCa_Vβ), and the Rat β subunit (rCavβ2) as an outgroup (**Figure 5C**). Sequence comparison across all amino acid positions revealed that the N-terminus exhibited the greatest sequence diversity (**Figure 5D**), consistent with previous findings showing extensive alternative splicing in this region in other organisms (Helton and Horne, 2002; Helton et al., 2002; Takahashi et al., 2003; Foell et al., 2004; Vendel et al., 2006; Ebert et al., 2008; Buraei and Yang, 2010; Siller et al., 2022). We found that all cnidarian Ca_Vβs conferred voltage-gated currents when co-expressed with Ca_Vα and α2δ subunits and had relatively low voltage thresholds for inactivation compared with rat or EdCa_Vβ2 (**Figure 5E**, **5S1A**, **5S1B**). Importantly, swapping the N-termini of each cnidarian Ca_Vβ onto EdCa_Vβ2 was sufficient to shift voltage-dependent inactivation to more negative values (**Figure 5E**, **5S1C**). Thus, alternative splicing at the N-terminus could serve as a broad molecular mechanism for tuning Ca_V function. Collectively, these findings substantiate the importance of Ca_Vβ in modulating inactivation and suggest a mechanism that could dynamically regulate a small region of only one subunit in the Ca_V protein complex to tune complex stinging behavior.

Discussion

Collectively, our studies on cnidarian stinging, here and (Weir et al., 2020), reveal different behavior in the primarily predatory anemone *Nematostella* versus the symbiotic anemone *Exaiptasia*. This study used a combination of theory and experimentation to uncover the molecular basis of regulation of the divergent behavior of *Exaiptasia* that uses stinging primarily for defense. Indeed, *Exaiptasia* obtains a large fraction of its energy and nutrients from endosymbiotic algae (Muscatine et al., 1981; Shick and Dykens, 1984; Steen, 1988), thus reducing overall pressure to predate. This finding is consistent with a common ecological theme in which symbiotic relationships are established whereby one partner provides food and the other provides shelter and defense (Lehnert et al., 2012; Bucher et al., 2016). Therefore, it is plausible that synergistic selection drives higher investment in defensive structures to protect symbiotic species.

Our results demonstrate that molecular adaptations tune distinct stinging behavior: *Nematostella* $Ca_V\beta$ confers an unusually low threshold for inactivation, basally inhibiting nematocytes unless they are exposed to synergistic prey cues: chemical (hyperpolarizing to relieve inactivation) and mechanical (depolarizing to recruit available Ca_V channels and elicit stinging) (Weir et al., 2020). These physiological mechanisms reflect a stinging strategy suited to opportunistic predation by *Nematostella*, which burrow within shallow marshes and sting unsuspecting prey. Consistent with the predictions of optimal control theory, *Nematostella* increased stinging with starvation, suggesting that evolution has shaped its stinging response to maximize benefits for predation. In contrast, *Exaiptasia* nematocytes contain a functionally specialized splice variant of $Ca_V\beta$ to mediate high threshold voltage-dependent Ca_V inactivation, consistent with Ca_V channel availability to amplify depolarizing signals from rest and stinging in response to touch alone. Thus, *Exaiptasia* physiology is consistent with an indiscriminate stinging strategy for defense, necessary for survival in an exposed environment that facilitates endosymbiotic photosynthesis (Muscatine et al., 1981; Shick and Dykens, 1984; Steen, 1988). Consistent with the predictions of optimal control theory, *Exaiptasia* stinging was nearly independent of starvation, suggesting that evolution has shaped the stinging response to maximize benefits for defense. Using molecular information gleaned from analyzing these two cnidarians, we find that $Ca_V\beta$ variation across cnidarians mediates differences in voltage-dependent inactivation, which could contribute to differences in stinging behavior. Thus, our study provides an example by which alternative splicing could account for adaptation across this diverse plethora of organisms and habitats.

While theory predicts robust trends for optimal predation and defense independent of environment, the precise nature of the predicted behavior does depend on the environment. In vivo, stinging is likely influenced by stimulus identity and intensity, background turbulence, and other factors. For example, cnidarians may have evolved distinct innate responses for different prey and use chemical sensing to enact the appropriate stinging response. In this case, optimal control theory can be used to predict the optimal response to known salient environmental cues. Alternatively, cnidarians may learn that specific prey are palatable and easy to catch through repeated exposure (Botton-Amiot et al., 2023). In this example, optimal control theory must be replaced by reinforcement learning as the likelihood of successful predation and its cost and benefits (the environment) are unknown (Sutton and Barto, 2018).

Indeed, stinging is a complex process mediated by numerous molecular components and cell types that could be subject to evolutionary change or acute modulation. Cnidarians occupy diverse ecological niches and experience varying metabolic demands, predatory challenges, and other survival pressures that could influence stinging behavior. Beyond cnidarians with stationary lifestyles that support photosynthetic endosymbionts (symbiotic anemones, corals, sea pens) and those that use opportunistic “sit-and-wait” ambush predatory strategies (burrowing anemones, siphonophores), others have evolved mobile lifestyles to actively capture prey (jellyfish) (Muscatine et al., 1981; Shick and Dykens, 1984; Steen, 1988; Fraune et al., 2016; Damian-Serrano et al., 2022). Stinging by mobile cnidarians could be subject to different physical demands, such as mechanical disturbance from increased turbulence that could necessitate distinct molecular control. Furthermore, stinging can be influenced by acute factors such as physiological state and various sensory cues, including chemicals, touch, or light (Pantin, 1942; Giebel et al., 1988;

Thorington and Hessinger, 1988; Watson and Hessinger, 1989; Plachetzki et al., 2012; Ozment et al., 2021; Aguilar-Camacho et al., 2023). Thus, further inquiry into modulation of stinging across physiological states such as nutritional condition, altered symbiotic relationships, or developmental stages (Sandberg et al., 1971; Columbus-Shenkar et al., 2018) could reveal dynamic regulation by synaptic connections, hormones, or modulation of transcriptional or

translational programs (Westfall et al., 1998, 2002; Westfall, 2004; Weir et al., 2020). Importantly, across all these scenarios, nematocytes remain single-use cells, so it is essential that signaling cascades control discharge in response to the most salient environmental stimuli. Overall, this study demonstrates how studying evolutionary novelties like stinging behavior can yield broad insight into signal transduction and cellular decision making.

Materials and Methods

Animals and Cells

Starlet sea anemones (*Nematostella vectensis*) were provided by the Marine Biological Laboratory (Woods Hole, Massachusetts). Adult animals of both sexes were used and kept on a 14 hr light/10 hr dark cycle at 26°C in 1/3 natural sea water (NSW). *Exaiptasia spp.* were purchased through Carolina Biological Supply Company (Cat #162865). Adult animals of both sexes were used following being kept on either a 10 hr light/14 hr dark cycle at 26°C in natural sea water (NSW) or a 14 hr light/10 hr dark cycle at 26°C in natural sea water (NSW). *Cassiopea spp.* were purchased through Carolina Biological Supply Company (Cat #162936). Unless stated otherwise, all animals were fed freshly hatched brine shrimp (Artemia) twice a week.

Exaiptasia diaphana were bleached through chemical methods (menthol-induced). Menthol (100mM in 100% ethanol; Sigma-Aldrich) was added to NSW at a final concentration of 0.2mM (Matthews et al., 2016). The anemones were incubated in the menthol/NSW treatment solution for a maximum of 8hr per day and outside of treatments anemones were incubated in NSW. For 2 weeks, anemones were treated 4 days per week and kept in the dark continuously starting from day 1 of treatment, aside from treatment changes. Animals were fed with Artemia approximately twice per week between bleaching treatments, enabling successful bleaching with minimal mortality. Their symbiotic status was assessed via fluorescence microscopy at the end of each week. For starvation experiments, animals were fed to excess for 1-2 weeks before the trial and withheld food entirely during the trial period and given water changes twice a week.

Nematostella nematocytes were isolated from tentacle tissue, which was harvested by anesthetizing animals in high magnesium solution containing (mM): 140 NaCl, 3.3 Glucose, 3.3 KCl, 3.3 HEPES, 40 $MgCl_2$. Cells were isolated from tentacles immediately prior to electrophysiology experiments by treatment with 0.05% Trypsin at 37°C for 15-20 min and mechanical dissociation in divalent free recording solution (mM): 140 NaCl, 3.3 Glucose, 3.3 KCl, 3.3 HEPES, pH 7.6. Dissociated cells were held on ice until use. Basitrichous isorhiza nematocytes were isolated from tentacles and identified by the presence of a capsule with high refractive index containing a barbed thread, oblong shape, and the presence of a cnidocil. *Exaiptasia* nematocytes were isolated from tentacle tissue immediately prior to electrophysiology experiments by incubation in a heat shock dissociation solution with (in mM): 430 NaCl, 10 KCl, 150 sucrose, 5 NaEGTA, 10 HEPES, 10 glucose, pH 7.6 at 45°C for 15-20 min and mechanical dissociation in the same solution. Dissociated cells were held on ice until use. Nematocytes were isolated from tentacles and identified by the presence of a capsule with high refractive index, oblong shape, and the presence of one or multiple apical cilia.

HEK293T cells (ATCC) were grown in Dulbecco's Modified Eagle Medium (DMEM) (Gibco) supplemented with 10% fetal calf serum (Gibco) and 50 I.U./mL penicillin and 50 µg/mL streptomycin (Gibco) at 37°C, 5% CO2 using standard techniques. For transfection, HEK293 cells were washed with Opti-MEM Reduced Serum Media (Gibco) and transfected using

lipofectamine 2000 (Invitrogen/Life Technologies Cat #11668019) according to the manufacturer's protocol. 1 µg each of *M. musculus* (mouse) *cacna1a* and rat *cacna2d1* and one of a wide variety of beta subunits (*Nematostella vectensis cacnb2.1* (NveCa$_V$β)*, Rattus norvegicus* (rat) *cacnb2a* (rCa$_V$β2)*, Exaiptasia diaphana* Ca$_V$βs (EdCa$_V$β1, EdCa$_V$β2)*, Cyanea capillata* Ca$_V$β (CcCa$_V$β)*, Physalia physalis* Ca$_V$β (PpCa$_V$β)*, Clytia hemisphaerica* Ca$_V$β (ChCa$_V$β)*, Cassiopea xamachana* Ca$_V$β (CxCa$_V$β2)) were coexpressed with 0.5 µg eGFP. We also assayed an array of different EdCa$_V$β2 mutants with N-termini from different animals by coexpressing 0.5 µg eGFP, 1 µg of *M. musculus* (mouse) *cacna1a* and rat *cacna2d1*, and one of a variety of beta subunits (*Nematostella vectensis cacnb2.1* mutant (NveCa$_V$β-N)*, R. norvegicus* (rat) *cacnb2a* mutant (rCa$_V$β-N)*, Exaiptasia diaphana* Ca$_V$β mutants (EdCa$_V$β1-N, EdCa$_V$β2-N)*, Cyanea capillata* Ca$_V$β mutant (CcCa$_V$β-N)*, Physalia physalis* Ca$_V$β mutant (PpCa$_V$β-N)*, Clytia hemisphaerica* Ca$_V$β mutant (ChCa$_V$β-N)*, Cassiopea xamachana* Ca$_V$β mutant (CxCa$_V$β2-N)). To enhance channel expression, cells were incubated with transfection mix containing plasmid DNA and Lipofectamine 2000 in Opti-MEM for 6 hr at 37°C. Cell were then re-plated on coverslips, incubated for 1-2 hr at 37 °C, and then incubated at 30°C for 2-6 days before experiments. Rat *cacna2d1 (*RRID: Addgene_26575) and *cacna1a* were gifts from D. Lipscombe (RRID: Addgene_26578) and *cacnb2a* was a gift from A. Dolphin (RRID: Addgene_107424).

Molecular biology

RNA was prepared from tentacles, body, and acontia tissues of WT and bleached adult *Exaiptasia* using published methods (Stefanik et al., 2013). Each tissue was homogenized (Millipore Sigma Cat #Z359971) and RNA was extracted using TRIzol Reagent (Thermo Fisher Cat #15596026), then after skipping the salt precipitation steps, RNA was purified and concentrated with the RNA Clean & Concentrator-5 kit (Zymo Research). For ddPCR experiments, droplet generation (QX200™ Droplet Generator BioRad Cat #1864002) and transfer of droplets to ddPCR™ 96-Well Plates (Bio-Rad Cat #12001925) were performed according to manufacturer's instructions (Instruction Manual, QX200™ Droplet Generator – Bio-Rad). Custom primers and probes and One-Step RT-ddPCR Advanced Kit for Probes (Bio-Rad Cat #1864021) reaction reagents and Droplet Generation Oil for Probes (Bio-Rad Cat #1863005) were sourced from Bio-Rad (see Key Resources Table for primer and probe sequences). The ddPCR plate was sealed with a Pierceable Foil Heat Seal (Bio-Rad Cat #1814040) and the PX1™ PCR Plate Sealer (Bio-Rad Cat #1814000). Plates were transferred to a Bio-Rad Thermalcycler C1000 (Bio-Rad Cat #1851197). The cycling protocol was the following: 45°C reverse transcription step for 60 minutes, 95°C enzyme activation step for 10 minutes followed by 40 cycles of a two-step cycling protocol (denaturation step of 95°C for 30 seconds and annealing/extension step of 58°C for 1 minute), 98°C enzyme deactivation step for 10 minutes, and holding at 12°C for an indefinite period before transfer to the QX200 Droplet Generator. The plates were read with the Bio-Rad QX200 Droplet Generator & Reader (Cat #1864003) and the RNA concentration per sample was processed using QuantaSoft (Bio-Rad Cat #1864011). Data were exported to Microsoft Excel and Prism (Graphpad) for further statistical analysis.

Most plasmids, including *Nematostella vectensis cacnb2.1* (NveCa$_V$β)*, Exaiptasia diaphana* Ca$_V$βs (EdCa$_V$β1, EdCa$_V$β2)*, Cyanea capillata* Ca$_V$β (CcCa$_V$β)*, Physalia physalis* Ca$_V$β (PpCa$_V$β)*, Clytia hemisphaerica* Ca$_V$β (ChCa$_V$β)*, Cassiopea xamachana* Ca$_V$β (CxCa$_V$β2))*, Nematostella vectensis cacnb2.1* mutant (NveCa$_V$β-N)*, R. norvegicus* (rat) *cacnb2a* mutant (rCa$_V$β-N)*, Exaiptasia diaphana* Ca$_V$β mutants (EdCa$_V$β1-N, EdCa$_V$β2-N)*, Cyanea capillata* Ca$_V$β mutant (CcCa$_V$β-N)*, Physalia physalis* Ca$_V$β mutant (PpCa$_V$β-N)*, Clytia hemisphaerica* Ca$_V$β mutant (ChCa$_V$β-N)*, Cassiopea xamachana* Ca$_V$β mutant (CxCa$_V$β2-N), were synthesized by Genscript (Piscataway, NJ). Sequence alignments were carried out using Clustal Omega. Wild type and Chimeric Ca$_V$β sequences are listed in **Supplemental Table 1**.

Cnidarian beta sequences were obtained from RNA sequencing or NCBI: *Nematostella vectensis cacnb2.1* (NveCa$_V$β) sequence (Weir et al., 2020), *Exaiptasia diaphana* Ca$_V$βs from RNA sequencing and confirmation from NCBI accession number KXJ28099.1 (EdCa$_V$β1) and NCBI accession number XP_020893045.1 (EdCa$_V$β2), *Cyanea capillata* Ca$_V$β (CcCa$_V$β) from NCBI accession number AAB87751.1 (Jeziorski et al., 1998), *Physalia physalis* Ca$_V$β (PpCa$_V$β) from NCBI accession number ABD59026 (Bouchard et al., 2006), *Clytia hemisphaerica* Ca$_V$β (ChCa$_V$β) from the MARIMBA database (Leclère et al., 2019), *Cassiopea xamachana* Ca$_V$β (CxCa$_V$β2) from RNA sequencing as TRINITY_DN5778_c3_g1_i5.p1.

Transcriptomics

Exaiptasia were anesthetized in 15% $MgCl_2$ NSW solution in a dish surrounded by an ice bath for 15 minutes. Tentacle, body, and acontia tissue were dissected and flash frozen in the presence of liquid nitrogen. *Cassiopea xamachana* were anesthetized in 10% $MgCl_2$ NSW solution in a dish surrounded by an ice bath for 15-20 minutes. Oral arms, bell, and cassiosome tissues were dissected and flash frozen in the presence of liquid nitrogen. All tissues were stored at −80°C until RNA extraction, library preparation, and RNA sequencing was performed by Genewiz (Azenta) using a HiSeq (2×150 bp) platform. Reads were examined for base quality distribution, kmer frequencies and adapter contamination by position in the read using fastqc (The Babraham Institute Bioinformatics Group), then where relevant, Rcorrector was used to remove erroneous k-mers (Song and Florea, 2015) and the FilterUncorrectablePEfastq python script from the Harvard Informatics group was used to discard read pairs. TrimGalore (The Babraham Institute) was then used to remove adapter contamination in reads and where relevant, Bowtie2 (Langmead and Salzberg, 2012) was used to remove reads originating from rRNA and Trinity was used to assemble reference transcriptomes *de novo* (Grabherr et al., 2011). Transdecoder was used to identify open reading frames (Haas, BJ) and Diamond used to annotate the transcriptome (Buchfink et al., 2015). Reads were pseudo-aligned and transcript abundance (TPM) was quantified using Kallisto (Bray et al., 2016) and our novel transcriptome assemblies as a reference and visualization and alignments were performed with Geneious Prime software and/or Clustal Omega (Madeira et al., 2022).

Electrophysiology

Recordings were carried out at room temperature using a MultiClamp 700B amplifier (Axon Instruments) and digitized using a Digidata 1550B (Axon Instruments) interface and pClamp software (Axon Instruments). Whole-cell recording data were filtered at 1kHz and sampled at 10kHz. Ca$_V$ activation data were leak-subtracted online using a p/4 protocol, and all membrane potentials were corrected for liquid junction potentials.

For whole-cell nematocyte recordings, borosilicate glass pipettes were polished to 8-10MΩ for *Nematostella* and 4-6MΩ for *Exaiptasia*, respectively. The standard *Nematostella* medium was used as the extracellular solution and contained (in mM): 140 NaCl, 3.3 glucose, 3.3 KCl, 3.3 HEPES, 2 $CaCl_2$, 0.5 $MgCl_2$, pH 7.6, 260-280mOsm. The standard *Exaiptasia* medium was used as extracellular solution and contained (in mM): 430 NaCl, 10 KCl, 10 $CaCl_2$, 50 $MgCl_2$, 10 HEPES, pH 7.6, 800-900mOsm. The intracellular solution for both *Nematostella* and *Exaiptasia* contained (in mM): isolating inward currents (in mM): 500 cesium methanesulfonate, 4 $MgCl_2$, 10 CsEGTA, 10 HEPES, 30 sucrose, pH 7.6, 260-280mOsm for *Nematostella* and 800-900mOsm for *Exaiptasia*. For *Nematostella* nematocyte recordings, voltage-dependent inactivation was measured during a 200ms activating pulse of −20mV following a series of 1s pre-pulses ranging from −110mV to 30mV, holding at −110mV. Voltage-gated currents were measured through a series of 200ms voltage pulses in 10mV

increments from −110mV to 70mV, holding at −110mV. For *Exaiptasia* nematocyte recordings, voltage-dependent inactivation was measured during a 200ms activating pulse of 0mV following a series of 1s pre-pulses ranging from −110mV to 30mV, holding at - 110mV. For both *Nematostella* and *Exaiptasia,* voltage-gated currents were measured through a series of 200ms steps 200ms voltage pulses in 10mV increments from −110mV to 70mV, holding at −110mV. For Cd^{2+} experiments, 500µM Cd^{2+} (dissolved in water) was applied locally and voltage-dependent activation was assessed through a single 200ms step to 0mV from a holding potential of −110mV.

For whole-cell recordings in HEK293 cells, pipettes were 3-6MΩ. The standard extracellular solution contained (in mM): 140 NaCl, 5 KCl, 10 HEPES, 2 $CaCl_2$, 2 $MgCl_2$, 10 Glucose, pH 7.4, 300-310mOsm. The intracellular solution contained (in mM): 5 NaCl, 140 cesium methanesulfonate, 1 $MgCl_2$, 10 EGTA, 10 HEPES, 10 sucrose, pH 7.2, 300-310mOsm. For Ca^{2+} currents in heterologously expressed channels, voltage-dependent inactivation was measured in one of two ways: (1) during an activating pulse of 0mV following a series of 1s pre-pulses ranging from −110mV to 50mV and holding potential of −80mV; or (2) during an activating pulse of 0mV following a series of 1s pre-pulses ranging from −110mV to 80mV and holding potential of −90mV. Voltage-gated Ca^{2+} currents were measured in response to 200ms voltage pulses in 10mV increments from −130mV to 80mV with −110mV holding potential. Voltage-dependent inactivation was quantified as I/I_{max}, with I_{max} occurring at the voltage pulse following a −110mV prepulse. In some instances, inactivation curves could not be fitted with a Boltzmann equation and were instead fitted with an exponential. G-V relationships were derived from I-V curves by calculating G: $G=I_{CaV}/(V_m- E_{rev})$ and fit with a Boltzmann equation. Data was processed and analyzed in Clampfit (pClamp 11 Software Suite, Molecular Devices) and Microsoft Excel and Prism (GraphPad).

In situ hybridization (BaseScope)

Adult *Exaiptasia* were paralyzed in anesthetic solution (15% $MgCl_2$), rinsed in PBS, then embedded in Tissue-Tek O.C.T. Compound (Sakura Cat #4583) in cryomolds (Sakura Tissue-Tek® Cryomold®, Intermediate, Cat #4566) and flash frozen on dry ice and stored at −80°C. Cryostat sections (18-20µm) were adhered to Fisherbrand™ Superfrost™ Plus Microscope Slides (Fisher Scientific Cat #12-550-15) and flash frozen on dry ice and stored at −80°C until used for BaseScope. The BaseScope Duplex Detection Reagent Kit (Advanced Cell Diagnostics Cat #323800) and the manufacturer's manual (BaseScope Duplex Detection Reagent User Manual, ACDBio) was followed to hybridize custom probes or positive control (Cat #700101) or negative control probes (Cat #700141) to targets in tissue cryosections and amplify signals. Samples were imaged on an Olympus BX41 Phase Contrast & Darkfield Microscope (Olympus Cat #BX41- PH-B) and images were acquired using the Olympus CellSens software and Olympus DP25 5MP Color Firewire Camera.

Behavior

Discharge of nematocysts was assessed based on well-established assays (Gitter et al., 1994; Watson and Hessinger, 1994; Weir et al., 2020). For assaying discharge, 5 mm round coverslips were coated with a solution of 25% gelatin (w/v) dissolved in NSW (for *Exaiptasia*) or 1/3 NSW (for *Nematostella*) and allowed to cure 3-4 hr prior to use. Coverslips were presented to the animal's tentacles for 5 seconds and then immediately imaged at 20X magnification using a transmitted light source. To assay behavioral responses to prey-derived chemicals, freshly hatched brine shrimp were flash frozen and ground to a powder with a mortar and pestle (Fisherbrand), then filtered through a 0.22µm syringe filter (VWR Cat #28145-501) and osmolarity adjusted for the specific anemone species. Coverslips were submerged in prey extract for 10 seconds then immediately presented to the animal.

Nematocytes visualized on coverslips were only those that embedded in the gelatin after discharge. For experiments using pharmacological agents such as $CdCl_2$, coverslips were submerged in a solution of 1M (*Exaiptasia*) or 10mM (*Nematostella*) Cd^{2+} in milli-Q water for 10 seconds then immediately presented to the animal. After performing the experiments, the animals were given several water changes to remove Cd^{2+}. Experiments carried out in the absence of extracellular Ca^{2+} were nominally Ca^{2+} free and did not include use of extracellular chelators. The region of the highest density of discharged nematocytes on the coverslip was imaged at 20X. Images were acquired with MetaMorph Microscopy Automation and Image Analysis Software (Molecular Devices) and the number of discharged nematocysts was counted by eye. Images were processed in Fiji (ImageJ) (Schindelin et al., 2012). *Exaiptasia* and *Nematostella* tentacles were examined by cutting a small portion of exposed tentacles and sandwiched between glass coverslips and then imaged at 20X with the MetaMorph software.

Phylogenetic and Genomic analyses

To infer exon boundaries and isoforms, we aligned Cav1 (NCBI accession number LJWW01000015.1) and Cav2 (NCBI accession number XM_021037386.2) to the *Exaiptasia diaphana* reference genome (BioProject PRJNA261862) (Baumgarten et al., 2015) using GMAP version 2015-07-23 (Wu and Watanabe, 2005). For phylogenetic analyses, we aligned nucleotide sequences with MAFFT v.7 (Katoh and Standley, 2013). We used ModelFinder (Kalyaanamoorthy et al., 2017) to assess the best model of substitution for phylogenetic inference. We estimated a maximum likelihood gene tree in IQ-TREE v2.0 (Minh et al., 2020). Support for clades was calculated using ultrafast bootstrap approximation UFBoot2 (Hoang et al., 2018). Percentage of identity for amino acids was calculated in overlapping windows.

Mathematical model: Optimal control theory for the stinging response

To model *Nematostella,* we assume the agent stings for predation. We thus introduce the state of satiation, s, that ranges from 0 to 1; at $s = 0$ the agent is most satiated and at $s = 1$ the agent is most starved. At each time step, the agent decides to perform an action (sting), a, representing the intensity of the attack; a ranges from 0 to 1, and is experimentally compared to the fraction of nematocytes fired in the behavioral assay. Each action has a cost that is proportional to the fraction of nematocysts that are fired, $c(a) = c_0 a$ where c_0 is the cost of discharging all nematocysts at once, or cost of full discharge, and we consider $c_!$ constant. Each stinging event has a probability $p(a)$ of achieving successful predation, where $p(a)$ increases with a (more intense attacks are more costly and more likely to succeed). A successful attack leads to the transition to the next state s' where the agent is more satiated $s \rightarrow s' = s - 1$ whereas a failed attack leads to higher starvation state $s \rightarrow s' = s + 1$. The most starved state is absorbing, which is equivalent to a point of no return. A reward $r(s')$ is assigned to the state of satiation reached upon attack, indicating its desirability ($r(s')$ is a decreasing function of s'), and the most starved state entails a starvation penalty $r(1) < 0$. Without loss of generality, all costs and rewards are normalized to the penalty of starvation, hence penalty of starvation is $r(1) = -1$. Our goal is to choose actions that maximize the expected sum of all future net rewards (reward - cost) for each state, which is called the value function. As customary in infinite horizon problems, we ensure convergence of the value function by introducing an effective horizon, i.e. by discounting exponentially rewards that are further in the future with a discount rate $\gamma < 1$.

The optimal value of a state, $V^*(s)$ and the corresponding optimal action $a^*(s)$ are obtained by solving the Bellman Optimality equation (Bellman, 2003).

$$V^*(s) = \max_a(p(a)\big(r(s-1) - c(a) + \gamma V^*(s-1)\big) + (1-p(a))(r(s+1) - c(a) + \gamma V^*(s+1)) \quad (1)$$
$$a^*(s) = \operatorname*{argmax}_a(p(a)\big(r(s-1) - c(a) + \gamma V^*(s-1)\big) + (1-p(a))(r(s+1) - c(a) + \gamma V^*(s+1))$$

With the boundary condition $V^*(1) = 0$. We solve these equations numerically with the value iteration algorithm (Sutton and Barto, 2018) and analytically under the assumption that $a^*(s)$ varies slowly with s (details of the asymptotic method can be found in ***Supplementary Information***). The asymptotic solution reproduces well the numerical results (compare lines and symbols in Figure 2B right, where we used $c_0 = 1$ and $p = p_M(2 - a^2)$ and $p_M = 0.8$ and showcased three different functional forms for $r(s)$, $r(s) = 10\ tan^{-1}(1 - s)$; $r(s) = 5\ cos\left(\frac{s\pi}{2}\right)$ and $r(s) = 3 - 3s^2$). We also explored how well the asymptotic result can capture the trend of the numerical result by varying the parameters in these three different forms for the reward (SI). The approximate solution is used to demonstrate that the stinging response increases with starvation under broad conditions, i.e. as long as $r(s)$ and $p(a)$ are concave functions and c(a) is convex (see ***Supplementary Information***). To exemplify the importance of acting optimally to save resources, we considered two agents, one acting optimally and one acting randomly i.e. shooting with a number of nematocysts uniformly distributed between $a_{\min}$ and a_{max}. Both agents start at the same starvation state ($s = 0.9$ in **Figure 2C**) and use on average the same number of nematocysts, but the random agent reaches starvation typically in tens of steps, whereas the optimal agent converges to a steady state (around $s = 0.3$ in the figure) and hardly ever reaches severe starvation.

To model *Exaiptasia*, we assume the agent stings for defense, thus the associated Markov process models transitions between the states of safety, which we indicate with L, and danger, which we indicate with D. The state of satiation is not affected by stinging and instead is dictated by a separate process that relies on symbionts and which we do not model. Similar to the previous model, the agent chooses an action, a, representing the intensity of the attack. Each attack has a likelihood to succeed $p(a)$ and an associated cost $c(a) = c_0 a$ where c_0 is the cost of full discharge of all nematocysts at once. A successful attack allows the animal to remain in state L and receive a unit reward; a failed attack leads to state D and penalty −1. F is an absorbing state hence $V^*(F) = 0$. The optimal value and action in state L follow:

$$V^*(L) = \max_a(p(a)(-c_0 a + \gamma V^*(L) + 1) + (1-p(a))(-1 - c_0 a)) \quad (2)$$
$$a^*(L) = \operatorname*{argmax}_a(p(a)(-c_0 a + \gamma V^*(L) + 1) + (1-p(a))(-1 - c_0 a))$$

Zeroing the derivative of the argument on the r.h.s. of equation (2) leads to

$$-c_0 + p'(a^*)(\gamma V^*(L) + 2) = 0$$
$$V^*(L) = -c_0 a^* + p(a^*)(\gamma V^*(L) + 1) + (1 - p(a^*))$$

Here, $p(a)$ is the probability of success of action a, hence it goes from $p(0) = 0$ to $p(1) = p_M < 1$. Assuming a specific form $p = p_M a(2 - a)$ leads to the specific solution $a^* = K - \sqrt{K^2 - A}$ where $K = \frac{2-\gamma}{c_0\gamma}$ and $A = -\frac{1}{\gamma p_M} + 2K$. If c_0 is constant, there is a non-trivial optimal action as long as $c_0 < 2p_M(2 - \gamma)$ and clearly the optimal action does not depend on starvation (constant solution in Figure 2E, right, with $c_0 = 1$; $\gamma = 0.99$ and $p_M = 0.8$).

Stinging predators does not improve nutritional state, thus transitions among different starvation states are not modelled for defensive stinging, but instead rely heavily on symbionts. However, to capture subtle effects of starvation on defensive stinging, we note that the cost of discharging nematocysts may still depend parametrically on whatever state

of starvation the agent happens to be in. In this case, $c_0 = c_0(s)$ and under the assumption that the cost increases with starvation, we find that optimal defensive stinging always decrease with starvation, for any functional form of p (see ***Supplementary Information*** for more details). The result is exemplified in **Figure 2E** (solutions that vary with starvation) using three functional forms for $c_0(s)$: $c_0 = s$; $c_0 = 1 - (s - 1)^2$, and a third function obtained by fitting the experimental data as described in the ***Supplementary Information***. Hence for defensive stinging, the optimal strategy is either independent of starvation or may decrease with starvation.

Statistical analysis

Data were analyzed with Clampfit (Axon Instruments), Prism (GraphPad), or QuantaSoft (BioRad Laboratories) and are represented as mean ± sem. n represents independent experiments for the number of cells/patches or behavioral trials. Data were considered significant if $p < 0.05$ using paired or unpaired two-tailed Student's t-tests or one-or two-way ANOVAs. All significance tests were justified considering the experimental design and we assumed normal distribution and variance, as is common for similar experiments. Sample sizes were chosen based on the number of independent experiments required for statistical significance and technical feasibility.

Data availability

Deep sequencing data are available via the Sequence Read Archive (SRA) repository under the BioProject accession code PRJNA945904. All plasmids are available upon request. Further requests for resources and reagents should be directed to and will be fulfilled by the corresponding author, NWB (nbellono@harvard.edu).

Acknowledgements

We thank B. Walsh and P. Kilian for assistance with animal husbandry, A. Whipple and D. Loftus with guidance for ddPCR experiments, A. Grearson for illustrations and photographs, K. Koenig and M. Martindale, and the Marine Biological Laboratory for providing animals. We also thank the Harvard Center for Biological Imaging (RRID:SCR_018673), Histology Core at the Harvard Department of Stem Cell and Regenerative Biology, and The Bauer Core Facility at Harvard University for infrastructure and experimental support. This research was supported by grants to NWB from the New York Stem Cell Foundation, Searle Scholars Program, and the NIH (R35GM142697), fellowships to LH from NSF Graduate Research Fellowship Program and Physics of Living Systems (PoLS) Graduate Fellowship, grants to AS from the European Research Council (ERC) under the European Union's Horizon 2020 research and innovation programme (grant agreement No 101002724 RIDING), the Air Force Office of Scientific Research under award number FA8655-20-1-7028, and the National Institutes of Health (NIH) under award number R01DC018789.

Author Contributions

LH, CA, SK, KW, and NWB contributed to physiological studies. LH contributed to behavioral, histological, and molecular studies. LH and WV contributed to phylogenetic, transcriptomic, and genomic studies. YQ and AS contributed to mathematical modelling studies. All authors were involved with writing or reviewing the manuscript.

Competing Interests

The authors declare no competing financial interests.

Supplementary Information Text: Markov Decision Processes modeling defensive vs predatory stinging.

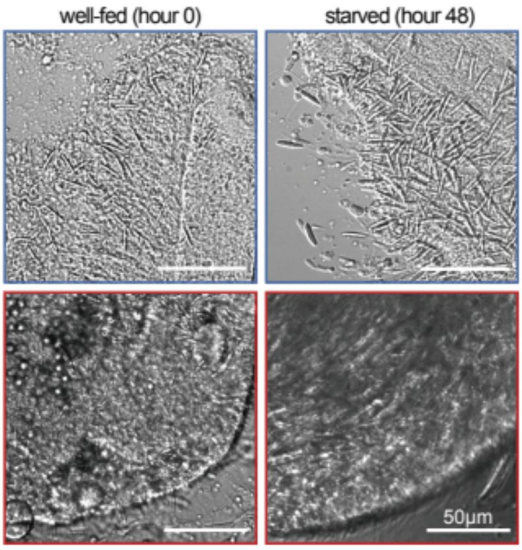

Figure 2S1.

Modulation of *Nematostella* and *Exaiptasia* stinging is not due to changes in the abundance of nematocytes.

Nematocytes were highly abundant in tentacles from *Nematostella (top)* and *Exaiptasia (bottom)* before and after starvation. Representative of n = 3 animals. Scale bar = 50µm.

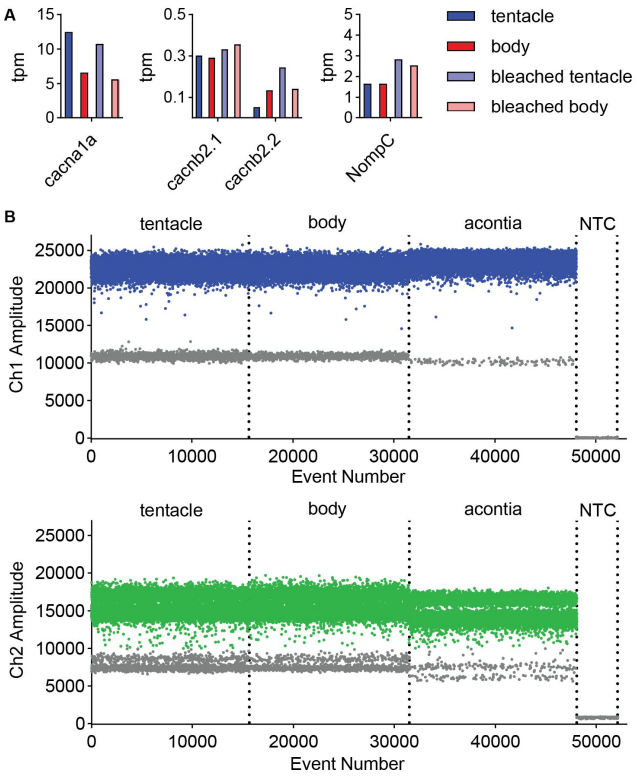

Figure 4S1.

Transcriptomic and molecular analyses of *Exaiptasia* β subunit isoforms.

A) mRNA expression (transcripts per million, TPM) of voltage-gated calcium (Ca_V) channel α and β subunits in *Exaiptasia* tentacle (nematocyte abundant, blue), body (nematocyte non-abundant, red), bleached (minimal symbionts) tentacle (light blue), bleached body (light red) tissues. NompC, the putative mechanoreceptor in *Nematostella* nematocytes (Schüler et al., 2015; Weir et al., 2020), was also detected in *Exaiptasia* tentacles.

B) Representative plots of fluorescent amplitude across event number (droplet events) from amplification of unique regions of EdCa_Vβ1 (Ch1, *Top*) and EdCa_Vβ2 (Ch2, *Bottom*) sequences using droplet digital PCR (ddPCR, Bio-Rad Laboratories). Individual lanes correspond to tentacle RNA, body RNA, acontia RNA, and no template control (NTC). Blue and green points indicate positive PCR droplets after thresholding and gray points indicate negative droplets.

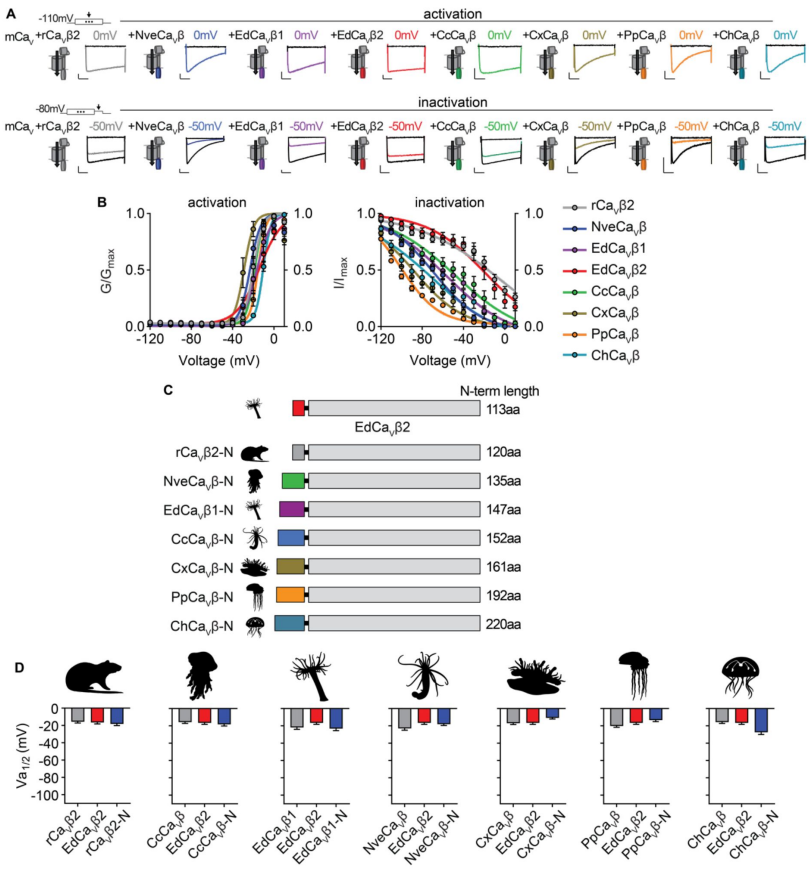

Figure 5S1.

Voltage-dependent activation of Ca_V channels is conserved across cnidarian β subunits.

A) *Top*: Voltage-gated currents from heterologously-expressed chimeric Ca_Vs with the indicated β subunits elicited by voltage pulses to −120mV (no current, black) and 0mV (colored). Abbreviations of species: Nve, *Nematostella vectensis*; Ed, *Exaiptasia diaphana*; Cc, *Cyanea capillata* (jellyfish); Pp, *Physalia physalis* (siphonophore); Ch, *Clytia hemisphaerica* (jellyfish); Cx, *Cassiopea xamachana* (jellyfish); r, *Rattus norvegicus*. *Bottom*: Voltage-gated currents elicited by a maximally activating voltage pulse following 1 s prepulses to −110 mV (max current, black), −50 mV (colored), or 20 mV (inactivated, no current, black). Scalebars = 100pA, 50ms.

B) Activation and inactivation curves for heterologously-expressed chimeric Ca_Vs with different β subunits. Activation: rCaVβ2 $V_{a1/2}$ = −19.76 ± 1.16mV, n = 12; NveCaVβ $V_{a1/2}$ = −23.07 ± 1.16mV, n = 5; EdCaVβ1 $V_{a1/2}$ = −18.27 ± 1.08mV, n = 8; EdCaVβ2 $V_{a1/2}$ = −14.22 ± 1.46mV, n = 5; CcCaVβ $V_{a1/2}$ = −18.47 ± 1.59mV, n = 6; CxCaVβ $V_{a1/2}$ = −28.89 ± 1.54mV, n = 15; PpCaVβ $V_{a1/2}$ = −15.29 ± 1.23mV, n = 10; ChCaVβ $V_{a1/2}$ = −10.30 ± 1.04mV, n = 12. rCaVβ2 $V_{i1/2}$ = −2.98 ± 13.51mV, n = 12; NveCaVβ $V_{i1/2}$ = −68.93 ± 1.53mV, n = 5; EdCaVβ1 $V_{i1/2}$ = −56.76 ± 3.18mV, n = 8; EdCaVβ2 $V_{i1/2}$ = −18.84 ± 8.00mV, n = 5; CcCaVβ subunit $V_{i1/2}$ = −47.81 ± 5.57mV, n = 6; CxCaVβ $V_{i1/2}$ = −87.75 ± 1.72mV, n = 15; PpCaVβ $V_{i1/2}$ = −99.80 ± 0.92mV, n = 10; ChCaVβ $V_{i1/2}$ = −70.25 ± 4.67mV, n = 12.

C) Diagram of Ca_V β subunit domain swaps and the length of the N-terminus swapped in amino acids.

D) Cnidarian Ca_V β N-termini do not greatly affect voltage-dependent activation of Ca_V channels containing EdCaVβ2. Voltage-dependent activation ($V_{a1/2}$) of heterologously-expressed Ca_Vs with WT EdCaVβ2, β subunits from the indicated cnidarians, and chimeras with their N-termini on EdCaVβ2, p = 0.5830 for average $V_{i1/2}$ values across mutant beta subunits, one-way ANOVA with Bartlett's test and post-hoc Tukey test, n = 4-7 cells. Data represented as mean ± sem.

Figure 5 Supplementary Table 1: Wild type and Chimeric Ca_Vβ amino acid sequences.

References

Aguilar-Camacho JM , Foreman K , Jaimes-Becerra A , Aharoni R , Gründer S , Moran Y (2023) **Functional analysis in a model sea anemone reveals phylogenetic complexity and a role in cnidocyte discharge of DEG/ENaC ion channels** *Commun Biol* **6**

Babonis LS , Enjolras C , Ryan JF , Martindale MQ (2022) **A novel regulatory gene promotes novel cell fate by suppressing ancestral fate in the sea anemone Nematostella vectensis** *Proc Natl Acad Sci* **119**

Babonis LS , Martindale MQ (2014) **Old Cell, New Trick? Cnidocytes as a Model for the Evolution of Novelty** *Integr Comp Biol* **54**:714–722

Baumgarten S , Simakov O , Esherick LY , Liew YJ , Lehnert EM , Michell CT , Li Y , Hambleton EA , Guse A , Oates ME , Gough J , Weis VM , Aranda M , Pringle JR , Voolstra CR (2015) **The genome of Aiptasia, a sea anemone model for coral symbiosis** *Proc Natl Acad Sci* **112**:11893–11898

Beckmann A , Özbek S (2012) **The Nematocyst: a molecular map of the Cnidarian stinging organelle** *Int J Dev Biol* **56**:577–582

Bedgood SA , Bracken MES , Ryan WH , Levell ST , Wulff J (2020) **Nutritional drivers of adult locomotion and asexual reproduction in a symbiont-hosting sea anemone Exaiptasia diaphana** *Mar Biol* **167**

Bellman R (2003) **Dynamic Programming**

Botton-Amiot G , Martinez P , Sprecher SG (2023) **Associative learning in the cnidarian Nematostella vectensis** *Proc Natl Acad Sci*

Bouchard C , Price RB , Moneypenny CG , Thompson LF , Zillhardt M , Stalheim L , Anderson PAV (2006) **Cloning and functional expression of voltage-gated ion channel subunits from cnidocytes of the Portuguese Man O'War Physalia physalis** *J Exp Biol* **209**:2979–2989

Bray NL , Pimentel H , Melsted P , Pachter L (2016) **Near-optimal probabilistic RNA-seq quantification** *Nat Biotechnol* **34**:525–527

Bucher M , Wolfowicz I , Voss PA , Hambleton EA , Guse A (2016) **Development and Symbiosis Establishment in the Cnidarian Endosymbiosis Model Aiptasia sp** *Sci Rep* **6**

Buchfink B , Xie C , Huson DH (2015) **Fast and sensitive protein alignment using DIAMOND** *Nat Methods* **12**:59–60

Buraei Z , Yang J (2010) **The β Subunit of Voltage-Gated Ca2+ Channels** *Physiol Rev* **90**:1461–1506

Columbus-Shenkar YY , Sachkova MY , Macrander J , Fridrich A , Modepalli V , Reitzel AM , Sunagar K , Moran Y (2018) **Dynamics of venom composition across a complex life cycle** *eLife* **7**

Damian-Serrano A , Hetherington ED , Choy CA , Haddock SHD , Lapides A , Dunn CW , Dam HG (2022) **Characterizing the secret diets of siphonophores (Cnidaria: Hydrozoa) using DNA metabarcoding** *PLOS ONE*

Darling JA , Reitzel AR , Burton PM , Mazza ME , Ryan JF , Sullivan JC , Finnerty JR (2005) **Rising starlet: the starlet sea anemone,Nematostella vectensis** *BioEssays* **27**:211–221

Ebert AM , McAnelly CA , Srinivasan A , Mueller RL , Garrity DB , Garrity DM (2008) **The calcium channel β2 (CACNB2) subunit repertoire in teleosts** *BMC Mol Biol* **9**

Foell JD , Balijepalli RC , Delisle BP , Yunker AMR , Robia SL , Walker JW , McEnery MW , January CT , Kamp TJ (2004) **Molecular heterogeneity of calcium channel β-subunits in canine and human heart: evidence for differential subcellular localization** *Physiol Genomics* **17**:183–200

Fraune S , Forêt S , Reitzel AM (2016) **Using Nematostella vectensis to Study the Interactions between Genome, Epigenome, and Bacteria in a Changing Environment** *Front Mar Sci 3*

Giebel GEM , Thorington GU , Lim RY , Hessinger DA (1988) **Control of Cnida Discharge: II. Microbasic p-Mastigophore Nematocysts are Regulated by Two Classes of Chemoreceptors** *Biol Bull* **175**:132–136

Gitter AH , Oliver D , Thurm U (1994) **Calcium-and voltage-dependence of nematocyst discharge in Hydra vulgaris** *J Comp Physiol A* **175**

Grabherr MG , et al. (2011) **Full-length transcriptome assembly from RNA-Seq data without a reference genome** *Nat Biotechnol* **29**:644–652

Grajales A , Rodríguez E (2014) **Morphological revision of the genus Aiptasia and the family Aiptasiidae (Cnidaria, Actiniaria** *Metridioidea). Zootaxa* **3826**

Helton TD , Horne WA (2002) **Alternative Splicing of the β 4 Subunit Has α 1 Subunit Subtype-Specific Effects on Ca 2+ Channel Gating** *J Neurosci* **22**:1573–1582

Helton TD , Kojetin DJ , Cavanagh J , Horne WA (2002) **Alternative Splicing of a b4 Subunit Proline-Rich Motif Regulates Voltage-Dependent Ca2+ Channels Gating and Toxin Block of Cav2** *J Neurosci* **22**:9331–9339

Hoang DT , Chernomor O , von Haeseler A , Minh BQ , Vinh LS (2018) **UFBoot2: Improving the Ultrafast Bootstrap Approximation** *Mol Biol Evol* **35**:518–522

Holstein T , Tardent P (1984) **An Ultrahigh-Speed Analysis of Exocytosis: Nematocyst Discharge** *Science* **223**:830–833

Jeziorski MC , Greenberg RM , Clark KS , Anderson PAV (1998) **Cloning and Functional Expression of a Voltage-gated Calcium Channel α1 Subunit from Jellyfish** *J Biol Chem* **273**:22792–22799

Kalyaanamoorthy S , Minh BQ , Wong TKF , von Haeseler A , Jermiin LS (2017) **ModelFinder: fast model selection for accurate phylogenetic estimates** *Nat Methods* **14**:587–589

Kass-Simon G (2002) **Scappaticci AA** *The behavioral and developmental physiology of nematocysts* **80**

Katoh K , Standley DM (2013) **MAFFT Multiple Sequence Alignment Software Version 7: Improvements in Performance and Usability** *Mol Biol Evol* **30**:772–780

Lam J , Cheng Y-W , Chen W-NU , Li H-H , Chen C-S , Peng S-E (2017) **A detailed observation of the ejection and retraction of defense tissue acontia in sea anemone (Exaiptasia pallida)** *PeerJ* **5**

Langmead B , Salzberg SL (2012) **Fast gapped-read alignment with Bowtie 2** *Nat Methods* **9**:357–359

Leclère L , et al. (2019) **The genome of the jellyfish Clytia hemisphaerica and the evolution of the cnidarian life-cycle** *Nat Ecol Evol* **3**:801–810

Lehnert EM , Burriesci MS , Pringle JR (2012) **Developing the anemone Aiptasia as a tractable model for cnidarian-dinoflagellate symbiosis: the transcriptome of aposymbiotic A. pallida** *BMC Genomics* **13**

Lubbock R , Amos WB (1981) **Removal of bound calcium from nematocyst contents causes discharge** *Nature* **290**:500–501

Lubbock R , Gupta BL , Hall TA (1981) **Novel role of calcium in exocytosis: mechanism of nematocyst discharge as shown by x-ray microanalysis** *Proc Natl Acad Sci* **78**:3624–3628

Madeira F , Pearce M , Tivey ARN , Basutkar P , Lee J , Edbali O , Madhusoodanan N , Kolesnikov A , Lopez R (2022) **Search and sequence analysis tools services from EMBL-EBI in 2022** *Nucleic Acids Res* **50**:W276–W279

Matthews JL , Sproles AE , Oakley CA , Grossman AR , Weis VM , Davy SK (2016) **Menthol-induced bleaching rapidly and effectively provides experimental aposymbiotic sea anemones (Aiptasia sp.) for symbiosis investigations** *J Exp Biol* **219**:306–310

Minh BQ , Schmidt HA , Chernomor O , Schrempf D , Woodhams MD , von Haeseler A , Lanfear R , Teeling E (2020) **IQ-TREE 2: New Models and Efficient Methods for Phylogenetic Inference in the Genomic Era** *Mol Biol Evol* **37**:1530–1534

Muscatine L , McCloskey L R. , Marian R E. (1981) **Estimating the daily contribution of carbon from zooxanthellae to coral animal respiration1: Muscatine et al** *Limnol Oceanogr* **26**:601–611

Nüchter T , Benoit M , Engel U , Özbek S , Holstein TW (2006) **Nanosecond-scale kinetics of nematocyst discharge** *Curr Biol* **16**:R316–R318

Östman C (2000) **A guideline to nematocyst nomenclature and classification, and some notes on the systematic value of nematocysts** *Sci Mar* **64**:31–46

Ozment E , Tamvacakis AN , Zhou J , Rosiles-Loeza PY , Escobar-Hernandez EE , Fernandez-Valverde SL , Nakanishi N (2021) **Cnidarian hair cell development illuminates an ancient role for the class IV POU transcription factor in defining mechanoreceptor identity** *eLife* **10**

Pantin CFA (1942) **Excitation of Nematocysts** *Nature* **3769**

Plachetzki DC , Fong CR , Oakley TH (2012) **Cnidocyte discharge is regulated by light and opsin-mediated phototransduction** *BMC Biol* **10**

Sandberg DM , Kanciruk P , Mariscal RN (1971) **Inhibition of Nematocyst Discharge correlated with Feeding in a Sea Anemone, Calliactis tricolor (Leseur)** *Nature* **232**:263–265

Schindelin J , Arganda-Carreras I , Frise E , Kaynig V , Longair M , Pietzsch T , Preibisch S , Rueden C , Saalfeld S , Schmid B , Tinevez J-Y , White DJ , Hartenstein V , Eliceiri K , Tomancak P , Cardona A (2012) **Fiji: an open-source platform for biological-image analysis** *Nat Methods* **9**:676–682

Schüler A , Schmitz G , Reft A , Özbek S , Thurm U , Bornberg-Bauer E (2015) **The Rise and Fall of TRP-N, an Ancient Family of Mechanogated Ion Channels, in Metazoa** *Genome Biol Evol* **7**:1713–1727

Shick JM , Dykens JA (1984) **Photobiology of the Symbiotic Sea Anemone Anthopleura elegantissima: Photosynthesis, Respiration, and Behavior under Intertidal Conditions** *Biol Bull* **166**:608–619

Siller A , Hofer NT , Tomagra G , Burkert N , Hess S , Benkert J , Gaifullina A , Spaich D , Duda J , Poetschke C , Vilusic K , Fritz EM , Schneider T , Kloppenburg P , Liss B , Carabelli V , Carbone E , Ortner NJ , Striessnig J (2022) **β2-subunit alternative splicing stabilizes Cav2.3 Ca2+ channel activity during continuous midbrain dopamine neuron-like activity** *eLife* **11**

Song L , Florea L (2015) **Rcorrector: efficient and accurate error correction for Illumina RNA-seq reads** *GigaScience* **4**

Steen G (1988) **The Bioenergetics of Symbiotic Sea Anemones (Anthozoa: Actiniaria)** *Symbiosis* **5**:103–142

Stefanik DJ , Wolenski FS , Friedman LE , Gilmore TD , Finnerty JR (2013) **Isolation of DNA, RNA and protein from the starlet sea anemone Nematostella vectensis** *Nat Protoc* **8**:892–899

Sutton Barto AG (2018) **Reinforcement learning: An introduction**

Takahashi SX , Mittman S , Colecraft HM (2003) **Distinctive Modulatory Effects of Five Human Auxiliary β2 Subunit Splice Variants on L-Type Calcium Channel Gating** *Biophys J* **84**:3007–3021

Tardent P (1995) **The cnidarian cnidocyte, a hightech cellular weaponry** *BioEssays* **17**:351–362

Thorington GU , Hessinger DA (1988) **Control of Cnida Discharge: I. Evidence for Two Classes of Chemoreceptor** *Biol Bull* **174**:163–171

Vendel AC , Terry MD , Striegel AR , Iverson NM , Leuranguer V , Rithner CD , Lyons BA , Pickard GE , Tobet SA , Horne WA (2006) **Alternative Splicing of the Voltage-Gated Ca2+ Channel β4 Subunit Creates a Uniquely Folded N-Terminal Protein Binding Domain with Cell-Specific Expression in the Cerebellar Cortex** *J Neurosci* **26**:2635–2644

Watson GM , Hessinger DA (1989) **Cnidocyte Mechanoreceptors are Tuned to the Movements of Swimming Prey by Chemoreceptors** *Science* **243**:1589–1591

Watson GM , Hessinger DA (1994) **Evidence for calcium channels involved in regulating nematocyst discharge** *Comp Biochem Physiol A Physiol* **107**:473–481

Watson GM , Mire-Thibodeaux P (1994) **The Cell Biology of Nematocysts** *International Review of Cytology, pp 275–300*

Weber J (1990) **Poly(gamma-glutamic acid)s are the major constituents of nematocysts in Hydra (Hydrozoa** *Cnidaria). J Biol Chem* **265**:9664–9669

Weir K , Dupre C , van Giesen L , Lee AS-Y , Bellono NW (2020) **A molecular filter for the cnidarian stinging response** *eLife* **9**

Westfall JA (2004) **Neural pathways and innervation of cnidocytes in tentacles of sea anemones** *Hydrobiologia* **530**

Westfall JA , Elliott CF , Carlin RW (2002) **Ultrastructural evidence for two-cell and three-cell neural pathways in the tentacle epidermis of the sea anemone Aiptasia pallida** *J Morphol* **251**:83–92

Westfall JA , Landers DD , McCallum JD (1998) **Different nematocytes have different synapses in the sea anemone Aiptasia pallida (Cnidaria** *Anthozoa). J Morphol* **238**:53–62

Wu TD , Watanabe CK (2005) **GMAP: a genomic mapping and alignment program for mRNA and EST sequences** *Bioinformatics* **21**:1859–1875

Author information

Lily S He
Department of Molecular and Cellular Biology, Harvard University, Cambridge MA 02138 USA

Yujia Qi
Machine Learning Center Genoa (MalGa), Department of Civil, Chemical and Environmental Engineering (DICCA), University of Genoa, Via Montallegro 1, 16145 Genoa, Italy

Corey AH Allard
Department of Molecular and Cellular Biology, Harvard University, Cambridge MA 02138 USA

Wendy A Valencia-Montoya
Department of Molecular and Cellular Biology, Harvard University, Cambridge MA 02138 USA, Department of Organismic and Evolutionary Biology and Museum of Comparative Zoology, Harvard University, Cambridge MA 02138 USA

Stephanie P Krueger
Department of Molecular and Cellular Biology, Harvard University, Cambridge MA 02138 USA

Keiko Weir
Department of Molecular and Cellular Biology, Harvard University, Cambridge MA 02138 USA

Agnese Seminara
Machine Learning Center Genoa (MalGa), Department of Civil, Chemical and Environmental Engineering (DICCA), University of Genoa, Via Montallegro 1, 16145 Genoa, Italy
For correspondence: agnese.seminara@unige.it

Nicholas W Bellono
Department of Molecular and Cellular Biology, Harvard University, Cambridge MA 02138 USA
For correspondence: nbellono@harvard.edu

Editors

Reviewing Editor
Leon Islas
Universidad Nacional Autónoma de México, Mexico

Senior Editor
Kenton Swartz
National Institute of Neurological Disorders and Stroke, National Institutes of Health, United States of America

Reviewer #1 (Public Review):

This manuscript by He et al. explores the molecular basis of the different stinging behaviors of two related anemones. The freshwater Nematostella which only stings when a food stimulus is presented with mechanical stimulation and the saltwater Exaiptasia which stings in response to mechanical stimuli. The authors had previously shown that Nematostella stinging is calcium-dependent and mediated by a voltage-gated calcium channel (VGCC) with very pronounced voltage-dependent inactivation, which gets removed upon hyperpolarization produced by taste receptors.

In this manuscript, they show that Exaiptacia and Nematostella differing stinging behavior is near optimal, according to their ecological niche, and conforms to predictions from a Markov decision model.

It is also shown that Exaiptacia stinging is also calcium-dependent, but the calcium channel responsible is much less inactivated at resting potential and can readily induce nematocyte discharge only in the presence of mechanical stimulation. To this end, the authors record calcium currents from Exaipacia nematocysts and discover that the VGCCs in this anemone

are not strongly inactivated and thus are easily activated by mechanical stimuli-induced depolarization accounting for the different stinging behavior between species. The authors further explore the role of the auxiliary beta subunit in the modulation of VGCC inactivation and show that different n-terminal splice variants in Exaiptacia produce strong and weak voltage-dependent inactivation.

The manuscript is clear and well-written and the conclusions are in general supported by the experiments and analysis. The findings are very relevant to increase our understanding of the molecular basis of non-neural behavior and its evolutionary basis. This manuscript should be of general interest to biologists as well as to more specialized fields such as ion channel biophysics and physiology.

Some findings need to be clarified and perhaps additional experiments performed.

1. The authors identify by sequencing that the Exaiptacia Cav is a P-type channel (cacna1a). However, the biophysical properties of the nematocyte channel are different from mammalian P-type channels. The cnidarian channel inactivation is exceedingly rapid and activation happens at relatively low voltages. These substantial differences should be mentioned and commented on.

2. The currents from Nematostella in Figure 3d seem to be poorly voltage-clamped. Poor voltage-clamp is also evident in the sudden increase of conductance in Figure 3C and might contribute to incorrect estimation of voltage dependence of activation and if present in inactivation experiments, also to incorrect estimation of the inactivation voltage range. This problem should be reassessed with new data.

3. While co-expression of the mouse Cav channel with the beta1 isoform from Exaiptacia indeed shifts inactivation to more negative voltages, it does not recapitulate the phenotype of the more inactivated Ca-currents in nematocytes (compare Figures 4d and 5d). It should be explained if this might be due to the use of a mammalian alpha subunit. Related to this, did the authors clone the alpha subunit from Exaiptacia? Using this to characterize the effect of beta subunits on inactivation might be more accurate.

4. The in situ shown in Figure 4b are difficult to follow for a non-expert in cnidarian anatomy. Some guidance should be provided to understand the structures. Also, for the left panels, is the larger panel the two-channel image? If so, blue would indicate co-localization of the two isoforms and there seems to be a red mark in the same nematocyte.

Reviewer #2 (Public Review):

This manuscript links the distinctive stinging behavior of sea anemones in different ecological niches to varying inactivation properties of voltage-gated calcium channels that are conferred by the identity of auxiliary Cavbeta subunits. Previous work from the Bellono lab established that the burrowing anemone, Nematostella vectensis, expresses a CaV channel that is strongly inactivated at rest which requires a simultaneous delivery of prey extract and touch to elicit a stinging response, reflecting a precise stinging control adapted for predation. They show here that by contrast, the anemone Exaiptasia diaphana which inhabits exposed environments, indiscriminately stings for defense even in the absence of prey chemicals, and that this is enabled by the expression of a CaVbeta splice variant that confers weak inactivation. They further use the heterologous expression of CaV channels with wild type and chimeric anemone Cavbeta subunits to infer that the variable N-termini are important determinants of Cav channel inactivation properties.

1. The authors found that Exaiptasia nematocytes could be characterized by two distinct inactivation phenotypes: (1) nematocytes with low-voltage threshold inactivation similar to that of Nematostella (Vi1/2 = ~ -85mV); and (2) a distinct population with weak, high-voltage threshold inactivation (Vi1/2 = ~ -48mV). What were the relative fractions of low-voltage and high-voltage nematocytes? Do the low-voltage Exaiptasia nematocytes behave similarly to Nematostella nematocytes with respect to requiring both prey extract and touch to discharge?

2. The authors state in Fig 3 legend and in the results that Exaiptasia nematocyte voltage-gated Ca2+ currents have weak inactivation compared with Nematostella. This description is imprecise and inaccurate. Figure 3 in fact shows that Exaiptasia nematocyte voltage-gated Ca2+ currents display a faster rate of inactivation compared to Nematostella Ca2+ currents. A sub-population of Exaiptasia nematocytes does display less resting state (or steady-state) inactivation compared to Nematostella Ca2+ currents. The authors need to be more accurate and qualify what type of inactivation property they are talking about.

3. In a similar vein, the authors need to be more accurate when referring to 'rat beta' used in heterologous expression experiments. It should be made explicit throughout the manuscript that the rat beta isoform used is rat beta2a. Among the distinct beta isoforms, beta2a is unique in being palmitoylated at the N-terminus which confers a characteristic slow rate of inactivation and a right-shifted voltage-dependence of steady-state inactivation consistent with the data shown in Fig. 4D. Almost all other rat beta isoforms do not have these properties.

4. The profiling of the impact of different Cnidarian Cavbeta subunits on reconstituted Ca2+ channel current waveforms is nice (Fig 5 and Fig 5S1). The N-terminus sequence of EdCaVβ2 is different from palmitoylated rat beta2a, though both have similar properties in showing slow inactivation and a right-shifted voltage-dependence of steady-state inactivation. Does EdCaVβ2 target autonomously the plasma membrane when expressed in cells? If so, this would reconcile with what was previously known and provide a rational explanation for the observed functional impact of the distinct Cavbetas.

Reviewer #3 (Public Review):

Summary:
The present article attempts to answer both the ultimate question of why different stinging behaviours have evolved in Cnidiarians with different ecological niches and shed light on the proximate question of which electro-physiological mechanisms underlie these distinct behaviours.

Account of major methods and results:
In the first part of the paper, the authors try to answer the ultimate question of why distinct dependencies of the sting response on internal starvation levels have evolved. The premise of the article that Exaiptasia's nematocyte discharge is independent of the presence of prey (Artemia nauplii) as compared to Nematostella's significant dependence of the discharge on the presence of actual prey, is shown be a robust phenomenon justified by the data in Figure 1.

The hypothesis that defensive vs. predatory stinging leads to different nematocyte discharge behaviours is analysed in mathematical models based on the suitable framework of optimal control/decision theory. By assuming functional relations between the:

1. cost of a full nematocyte discharge and the starvation level.

2. probability of successful predation/avoidance on the discharge level.

3. desirability/reward of the reached nutritional state.

Based on these assumptions of environmental and internal influences, the optimal choice of attack intensity is calculated using Bellman's equation for this problem. The model predictions are validated using counted nematocytes on a coverslip. The scaling of normalised nematocyte discharge numbers with scaled starvation time is qualitatively comparable to what is predicted from the models. The abundance of nematocytes in the tentacles was, on the other hand, independent of the starvation state of the animals.

Next, the authors turn to investigate the proximate cause of the differential stinging behaviour. The authors have previously reported convincing evidence that a strongly inactivating Cav2.1 channel ortholog (nCav) is used by Nematostella to prevent stinging in the absence of prey (Weir et al. 2020). This inactivation is released by hyperpolarising sensory inputs signalling the presence of prey. In this article, it is clearly shown by blocking respective currents that Exaiptasia, too, relies on extracellular $Ca2+$ influx to initiate stinging. Patch clamp data of the involved currents is provided in support. However, the authors find that in addition to the nCav with a low-inactivation threshold, Exaiptasia has a splice variant with a higher inactivation threshold expressed (Figure 3D).

The authors hypothesise that it is this high-threshold nCav channel population that amplifies any voltage depolarisation to release a sting irrespective of the presence of prey signals. They found that the β subunit that is responsible for Nematostella's unusually low inactivation threshold exists in Exaiptasia as two alternative splice isoforms. These N-terminus variants also showed the greatest variation in a phylogenetic comparison (Figure 5), rendering it a candidate target for mutations causing variation in stinging responses.

Appraisal of methodology in support of the conclusions:
The authors base their inference on a normative model that yields quantitative predictions which is an exciting and challenging approach. The authors take care in stating the model assumptions as well as showing that the data indeed does not contradict their model predictions. The interesting comparative nature of the modelling part of the study is complicated by slightly different cost assumptions for the two scenarios. Hence, Figure 2 needs to be carefully digested by readers.

It would be even more prudent to analyse the same set of cost-of-discharge vs. starvation scenarios for both species. Specifically, for Nematostella the complete cost-of-discharge vs starvation-state curves as for Exaiptasia (Figure 2E, example 2-4) could be used. It is likely that the differential effect size of Nematostella and Exaiptasia behaviour is the strongest if only the flat cost-of-discharge vs starvation is used (Figure 2A) for Nematostella. But as a worst-case comparison the other curves, where the cost to the animal scales with starvation would be a good comparison. This could help the reader to understand when the different prediction of Nematostella's behaviour breaks down. In addition, this minor change could shed light on broader topics like common trade-offs in pursuit predation.

The qualitatively similar scaling of the model-derived relation between starvation and sting intensity with the counted nematocytes for different feeding pauses is evidence that feeding has indeed been optimised for the two distinct ecological niches.
To prove that Exaiptasia uses a similar $Ca2+$ channel ortholog as well as a different splice variant, the authors employed both clean electrophysiological characterisaiton (Figure 3) as well as transcriptomics data (Figure 4S1).

To strengthen the authors' hypothesis that variation in the N-termini leads to changes in $Ca2+$ channel inactivation and hence altered stinging, the response sequence variability of 6

Cnidaria was analysed.

Additional context:
Although, the present article focuses on nematocytes alone, currently, there has been a refocus in neurobiology on the nervous systems of more basal metazoans, which received much attention already in the works of Romanes (1885). In part, this is driven by the goal to understand the early evolution of nervous systems. Cnidarians and Ctenophors are exciting model organisms in this venture. This will hopefully be accompanied by more comparative studies like the present one. Some of the recent literature also uses computational models to understand mechanisms of motor behaviour using full-body simulations (Pallasdies et al. 2019; Wang et al. 2023), which can be thought of as complementary to the normative modelling provided by the authors.

Comparative studies of recent Cnidarians, such as the present article, can shed light on speculative ideas on the origin of nervous systems (Jékely, Keijzer, and Godfrey-Smith 2015). During a time (the Ediacarium/Cambrium transition) that has seen the genesis of complex trophic foodwebs with preditor-prey interaction, symbioses, but also an increase of body sizes and shapes, multiple ultimate causes can be envisioned that drove the increase in behavioural complexity. The authors show that not all of it needs to be implemented in dedicated nerve cells.

References:

Jékely, Gáspár, Fred Keijzer, and Peter Godfrey-Smith. 2015. "An Option Space for Early Neural Evolution." Philosophical Transactions of the Royal Society B: Biological Sciences 370 (December): 20150181. https://doi.org/10.1098/rstb.2015.0181.

Pallasdies, Fabian, Sven Goedeke, Wilhelm Braun, and Raoul-Martin Memmesheimer. 2019. "From Single Neurons to Behavior in the Jellyfish Aurelia Aurita." eLife 8 (December). https://doi.org/10.7554/elife.50084.

Romanes, G. J. 1885. Jelly-Fish, Star-Fish and Sea-Urchins: Being a Research on Primitive Nervous Systems. Appleton.

Wang, Hengji, Joshua Swore, Shashank Sharma, John R. Szymanski, Rafael Yuste, Thomas L. Daniel, Michael Regnier, Martha M. Bosma, and Adrienne L. Fairhall. 2023. "A Complete Biomechanical Model of *hydra* Contractile Behaviors, from Neural Drive to Muscle to Movement." Proceedings of the National Academy of Sciences 120 (March). https://doi.org/10.1073/pnas.2210439120.

Weir, Keiko, Christophe Dupre, Lena van Giesen, Amy S-Y Lee, and Nicholas W Bellono. 2020. "A Molecular Filter for the Cnidarian Stinging Response." eLife 9 (May). https://doi.org/10.7554/elife.57578.